A MATHEMATICAL MODEL FOR HYDROGEN PRODUCTION FROM A PROTON EXCHANGE MEMBRANE PHOTOELECTROCHEMICAL CELL

A Thesis

Presented to

The Graduate Faculty of The University of Akron

In Partial Fulfillment

of the Requirements for the Degree

Master of Science

Bryan Richard Van Scoy

May, 2012

A MATHEMATICAL MODEL FOR HYDROGEN PRODUCTION FROM A PROTON EXCHANGE MEMBRANE PHOTOELECTROCHEMICAL CELL

Bryan Richard Van Scoy

Thesis

Approved:

Advisor
Dr. Gerald Young

Co-Advisor
Dr. Curtis Clemons

Faculty Reader
Dr. Kevin Kreider

Department Chair
Dr. Timothy Norfolk

Accepted:

Dean of the College
Dr. Chand Midha

Dean of the Graduate School
Dr. George Newkome

Date

ABSTRACT

A single-phase, one-dimensional, non-isothermal model is developed to describe the proton distribution, electric potential, water content, and temperature profile throughout a proton exchange membrane photoelectrolysis cell (PEM PEC). The anode catalyst layer, membrane, and cathode catalyst layer are modeled while the effects of the water channels are accounted for in boundary conditions. The Nafion membrane contains SO_3^- charges which are modeled by delta functions. The total current density is composed of the current due to electrolysis and the photocurrent caused by sunlight due to the photoelectric effect. Numerical techniques are implemented to solve the coupled partial differential equations describing the system. Results include predictions of the amount of hydrogen production along with steady-state distributions of protons, electric potential, water content, and temperature throughout the cell. Data are compared for various sets of parameters to a default case. Hydrogen production for the default case is 5.86 mL/min while values of up to 22.5 mL/min were obtained by increasing the size of the cell. Other variables studied include the number of SO_3^- and H^+ groups in the membrane, spacing of the charge groups, and sizes of the regions along with the effects of photocurrent, mobility, and temperature on hydrogen production.

ACKNOWLEDGEMENTS

I would like to acknowledge my advisors and faculty readers for all of their time, effort, and guidance that resulted in this work. Also, thank you to my friends and family for your support.

TABLE OF CONTENTS

LIST OF TABLES

LIST OF FIGURES

CHAPTER I

INTRODUCTION

1.1 Hydrogen Fuel

Natural resources currently being used for energy are being steadily depleted, increasing the need for an alternative source of energy. Action must be taken to search for alternative energies that are efficient, economical, and produce little or no harmful emissions. Hydrogen as an energy carrier is a current topic of research that shows much promise for the future. Although hydrogen is one of the most abundant substances in the universe, it rarely occurs as pure hydrogen and therefore must be produced. If hydrogen can be efficiently produced, then an economy based on hydrogen fuel may be possible. One advantage of a hydrogen economy is hydrogen's ability to be produced using a variety of naturally occurring resources such as natural gas, coal, biomass, waste, sunlight, wind, and nuclear power [2]. Such diversification allows for hydrogen to be produced in nearly every geographic region in a way that is most suited for the area. Hydrogen also has the benefit of significantly reducing urban pollution and greenhouse gas emissions compared to current fuels [3]. The amount of emissions depends on the way in which the hydrogen is produced, stored, and then used, although harmful pollutants can be eliminated in the production pro-

cess by producing hydrogen using electrolysis, the process of splitting water to form hydrogen and oxygen.

Proton exchange membrane photoelectrochemical cells (PEM PECs) harvest energy from sunlight and use it to electrolyze water, forming both hydrogen and oxygen gas. Much more research must be done, however, before photoelectrochemical cells become efficient enough to compete with current energy sources. Photoelectrochemical cells do show promise as researchers at the National Renewable Energy Laboratory in Golden, Colorado have produced hydrogen with 12% efficiency from sunlight [2]. The goal of this paper is to develop a mathematical model for a PEM PEC which will lead to useful insights to aid in cell design and to increase cell efficiency.

1.2 Physical Operation

The PEM PEC is composed of two water channels, two porous catalyst layers (CLs), and a proton exchange membrane (PEM). Water is pumped into the anode and cathode water channels which diffuses into the anode and cathode CLs. In the anode CL, the reaction

$$H_2O \Longleftrightarrow 2H^+ + 2e^- + 0.5O_2 \tag{1.1}$$

occurs. The electrons travel through an external circuit to the cathode CL, the oxygen gas is released, and the hydrogen protons travel through the PEM. The driving forces that transport the hydrogen across the PEM are drift caused by the externally supplied electric field and diffusion from the pile up of hydrogen at the anode.

The hydrogen and electrons then combine at the cathode CL to form hydrogen gas according to

$$2\mathrm{H}^+ + 2\mathrm{e}^- \Longleftrightarrow \mathrm{H}_2. \tag{1.2}$$

The hydrogen gas produced can then be captured and stored to be used as fuel for a device such as a fuel cell. A representative diagram of the processes in a photoelectrochemical cell can be found in Figure 1.1. The PEM performs a very important role

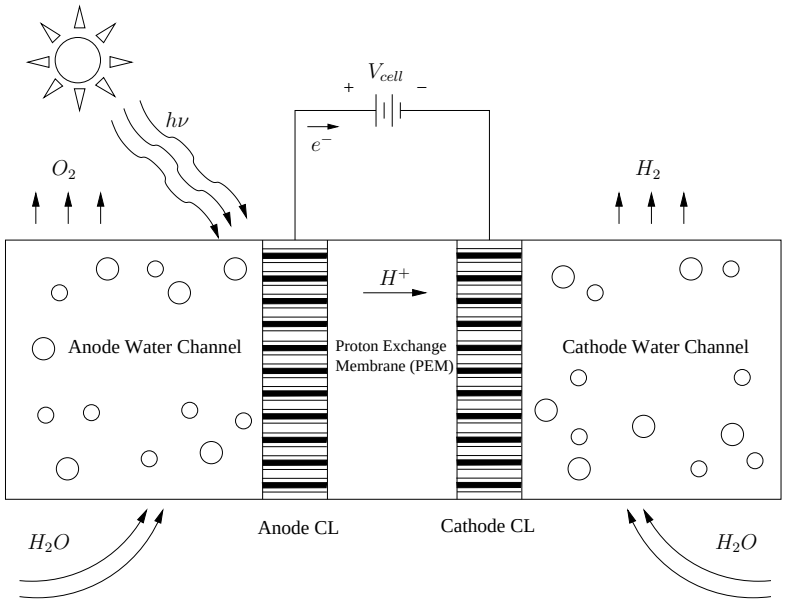

Figure 1.1: Schematic (not to scale) of the proton exchance membrane photoelectrochemical cell (PEM PEC).

in determining the efficiency of the cell since it must easily allow the protons to pass through the membrane. Otherwise, the hydrogen and oxygen recombine before the hydrogen gas is formed. A common polymer used for the PEM is Nafion due to its

intrinsic chemical and mechanical stability, high proton conductivity, and gas impermeability [4]. Nafion consists of a polymer backbone and perfluorinated vinyl ether side chains with a sulfonic acid group (SO_3H) at the end of each chain; see Figure 1.2 [5]. The role of the hydration shell is to prevent the protons from combining with the SO_3^- groups. The sulfonic acid groups and water molecules facilitate proton transport across the membrane, although exactly how this occurs is still largely unknown [6].

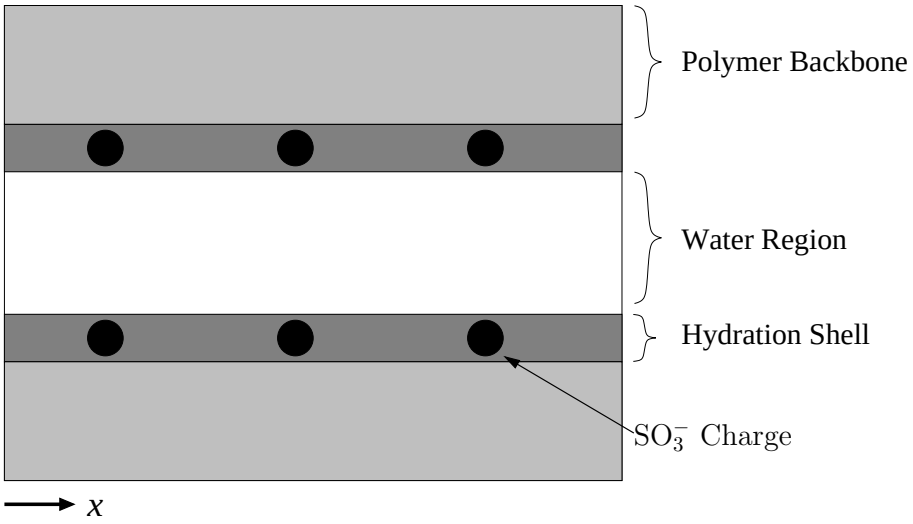

Figure 1.2: Structure of Nafion showing the SO_3^- groups in the hydration shell separating the polymer backbone and water region.

The anode and cathode electrode assemblies are composed of nanowire arrays which conduct protons and electrons. In the anode, the nanowires are composed of a silicon

(Si) core and germanium (Ge) shell while the cathode nanowires are opposite. This creates a pn-junction which acts as a solar cell, similar to a photodiode. Sun strikes the platinum catalyst which frees electrons as electrolysis occurs. The pn-junction in the anode causes the electrons to travel through the silicon nanowires to the conductive support scaffold. On the cathode side, the pn-junction is in the opposite direction which forces electrons to flow out of the nanowire arrays where they combine with hydrogen protons to form H_2 gas. The electrode nanowire assemblies are shown in Figure 1.3. Research is currently being done on these nanowire arrays in order to make them longer, more uniform, and more easily produced [7, 8, 9].

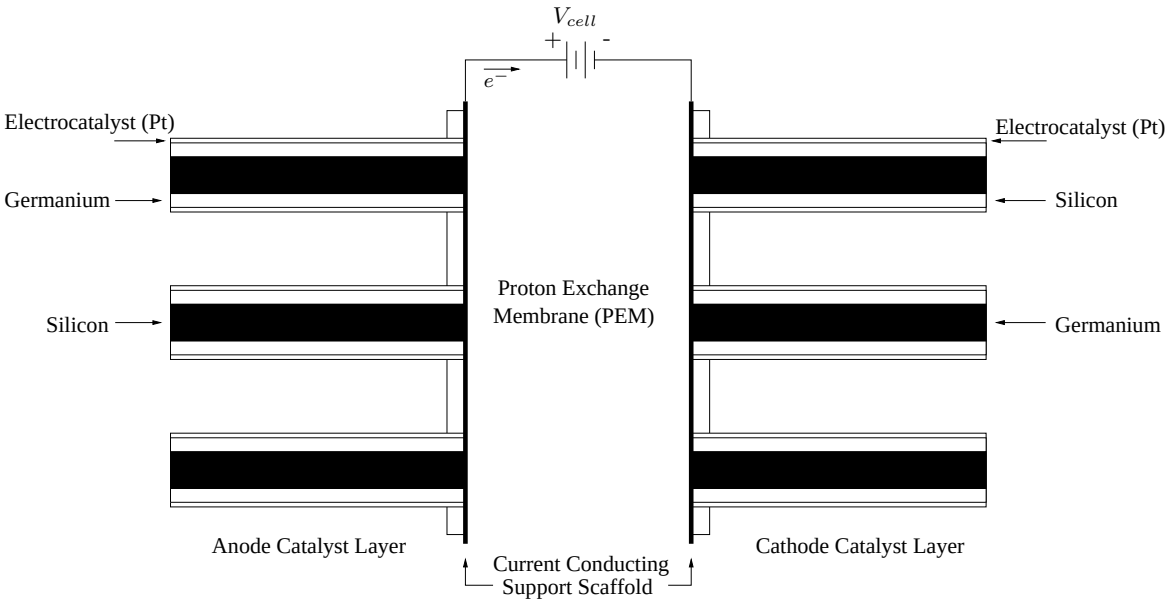

Figure 1.3: Electrode nanowire array assembly.

Our model is used to answer questions about the membrane and its effects on hydrogen production. This will by done by varying the number and distribution of the SO_3^- groups, sizes of the regions, amount of sunlight, proton mobility, cell temperature, and water content. In order to answer these questions, the proposed model tracks the concentration of protons, electrical potential, temperature, and water content throughout the catalyst layers and proton exchange membrane.

1.3 Previous Research

Although many studies have been done for PEM fuel cells, very little research has been done on PEM electrolysis cells. Since they are very similar, many of the results for fuel cells may be applied to electrolysis cells as long as caution is used to justify the results.

Nie et al. [4] develop a first-generation model to describe the current-potential characteristics of a photoelectrochemical cell based on charge and mass balances and Butler-Volmer kinetics at the electrodes. An equivalent circuit model is presented which describes the overall cell potential as the sum of the cell Nernst potential, anode, cathode and membrane overpotentials, and interfacial resistance. It is assumed that the regions are well mixed and that no transport limitations exist. Results show that the membrane resistance increases and the anode and cathode overpotentials increase with a decrease in temperature. The hydrogen production rate is found to increase by about 11% from operating temperature 30 °C to 80 °C.

Akinaga et al. [5] use the Lattice Boltzmann method (LBM) to solve for proton

transport in one channel of a two-dimensional structure proton exchange membrane of Nafion. The channel is assumed to be straight and cylindrical in shape. The effects of channel radius and distance between SO_3^- groups on the average mobility of protons are studied, where the channel width corresponds to the water content of the membrane. It is found that the average mobility of protons increases as the SO_3^- groups are spaced homogeneously throughout the channel and as the radius of the channel is increased. Also, the relative dielectric constant, or static permittivity, in Nafion may have a wide range of values from 2.0 - 78.0 depending on the position in the membrane with the center of the membrane behaving similar to that of bulk water. Since a two-dimensional model is used, the authors expect the resistance to proton motion to be underestimated due to the potential gradient being smaller than that of a three-dimensional system.

Paddison et al. [6] provide a review of previous atomistic studies of proton transport in Nafion. Protons in a water medium may travel not only by vehicular diffusion, but also by structural diffusion which is known as the Grotthuss shuttling mechanism. The latter is completely neglected by standard classical forces and must be taken into account. It is found that the Grotthuss mechanism actually opposes vehicular diffusion, reducing the net diffusion. Atomistic models are used to determine that water molecules are highly restricted near the sulfonate groups at low water contents, while the water molecules near the sulfonate groups are relatively mobile at high water contents. Investigations regarding the distribution of the sulfonate groups are also performed, and no reason is found to believe that the distribution of sulfonate

groups is not random, although random variations may be able to be exploited to improve membrane efficiency.

Due to their similarities in operation, useful insight may also be found for photoelectrochemical cells by studying the research done on fuel cells; see Du [10], Lee [11], Kang [12], and Chen [13]. Kreuer [14] for instance studies various polymers, including Nafion, to be used for the PEM of a fuel cell and the effects of temperature on the polymers. Desirable characteristics for the PEM include high acid contents in the sulfonic acid groups, well connected narrow channels, and blending or cross-linking of polymers for morphological stability. Nafion has a higher hydrophobic to hydrophilic separation which results in wider, more connected hydrophilic channels. For high temperature applications, heterocycles can be used as a proton solvent instead of water. These electrolytes have similar transport properties to that of water near their respective melting point which is unique to each heterocycle. Thus various solvents can be used depending on the desired operating temperature to achieve higher efficiencies.

Afshari et al. [15] develop a two-dimensional model for a PEM fuel cell to study the transport of water in the cell which is critical for proper hydration and cell efficiency. Water transport and the temperature distribution throughout the cell are solved as a set of coupled differential equations using conservation laws for mass, momentum, species, energy, and charge with electrochemical relations. A single-domain approach is used where each conservation law is applied to each of the various regions in the cell with appropriate boundary conditions between the regions. The model is two-phase

in that it accounts for gas and liquid flow. Steady-state flow of ideal gas mixtures and no contact resistance at the interfaces between layers are assumed. Results for single-phase and two-phase models are shown, displaying the slight variances in the models. In both cases, the temperature was found to be higher throughout the membrane than in the anode and cathode gas channels. The temperature distribution is highly sensitive to the cell voltage (chosen to be .55V) and is found to be the most important parameter affecting two-phase water transport. Simulations are also performed for isothermal and non-isothermal conditions. The non-isothermal conditions produce more accurate results, indicating that the rise in temperature in the membrane does have a noticeable impact on the cell performance.

1.4 Model and Assumptions

The proposed model solves for the hydrogen concentration, electric potential, temperature, and water content in the anode and cathode CLs and in the PEM. Limitations and assumptions of the model include the following:

1. The model is one-dimensional.
2. SO_3^- groups are evenly distributed.
3. Channel flow is linear.
4. Only steady-state analysis is considered.
5. Water channels are not modeled.

The rest of the paper is organized as follows. In Chapter II, the mathematical model for the photoelectrochemical cell is developed. Discretization of the governing equations is shown in Chapter III, followed by the presentation and discussion of results in Chapter IV. Chapter V concludes with a summary and proposed future work.

CHAPTER II

MATHEMATICAL MODEL

2.1 Governing Equations

The general conservation law written in differential form is given by

$$u_t + \nabla \cdot \vec{J} = S, \tag{2.1}$$

where u is the density, J is the flux, and S is the source/sink term. This form assumes sufficient smoothness of u and J on the domain. The assumption is validated by requiring continuity and continuity of flux between regions of the PEM PEC, and smoothness of the solution can be seen in plots in the following chapters. Since this model only solves for the steady-state solution, $u_t = 0$, so the general conservation equation reduces to

$$\nabla \cdot \vec{J} = S. \tag{2.2}$$

For reference, all of the nomenclature used throughout this paper is given in Tables 2.1 and 2.2.

Table 2.1: Nomenclature (Part I)

Symbol	Description	Symbol	Description
A	Surface area/volume ratio [m^{-1}]	pos	Position of point-charges
c	Speed of light [m/s]	q	Charge of a proton [C]
D	Diffusivity of protons [m^2/s]	R	Gas constant [J/K·mol]
D_w	Diffusivity of water [m^2/s]	S	Source/Sink term
E	Activation energy [J/mol]	T	Temperature [K]
EW	Equivalent weight of electrolyte [kg/mol]	W	Molecular weight [kg/mol]
F	Faraday constant [C/mol]	V	Volume [m^3]
h	Planck constant [m^2·kg/s]	V_0	Equilibrium potential [V]
I_ν	Radiant intensity [W/m^2]	η	Overpotential [V]
j	Current density [A/m^3]	μ	Mobility of protons [$m^2/V{\cdot}s$]
J	Flux	ρ	Density [kg/m^3]
k_B	Boltzmann constant [J/K]	κ	Thermal conductivity [W/m·K]
L	Length [m]	σ	Ionic conductivity [S/m]
m	Mass of an electron [kg]	ϵ	Permittivity [F/m]
N_A	Avogadro constant [mol^{-1}]	ν	Frequency of sunlight [Hz]
$N_{SO_3^-}$	Number of SO_3^- charges	χ	Surface potential difference [J]
n	Concentration of protons [mol/m^3]	ϕ_{metal}	Work function of metal [J]

Table 2.2: Nomenclature (Part II)

Symbol	**Description**	**Symbol**	**Description**
n_d	Electro-osmotic drag coefficient [mol H_2O/mol SO_3^-]	ϕ	Electric potential [V]
P	Pitch [m]	λ	Water content [mol H_2O/mol SO_3^-]

2.1.1 Hydrogen Concentration

The ultimate purpose of the PEM PEC is to produce hydrogen, so the hydrogen distribution throughout the cell is a crucial aspect of the cell model. In order to use equation (2.2), the flux and source terms must be determined. Using Fick's law of diffusion, the flux due to the diffusion of protons is

$$\vec{J} = -D\ \nabla n, \tag{2.3}$$

where D is the diffusivity of protons and n is the concentration of protons. The general form for the advective flux is

$$\vec{J} = \vec{v}\ n, \tag{2.4}$$

where $\vec{v}$ is the velocity of protons. The average velocity of protons can be expressed as

$$\begin{aligned} \vec{v}_{avg} &= \mu\vec{E} \\ &= \mu(-\nabla\Phi), \end{aligned} \tag{2.5}$$

where μ is the mobility of protons, $\vec{E}$ is the electric field, and Φ is the electric potential. Combining equations (2.3) - (2.5), the total flux of protons is

$$\vec{J} = -D\ \nabla n - \mu n\ \nabla \Phi. \tag{2.6}$$

The source term in the anode corresponds to the production of hydrogen from electrolysis according to equation (1.1) while the sink term in the cathode corresponds to the hydrogen protons combining to form H_2 according to equation (1.2). Using the electrolysis equations (1.1) and (1.2) and Faraday's law of electrolysis, the complete set of hydrogen concentration equations can then be written as

$$\begin{aligned} 0 &= \nabla \cdot (D\ \nabla n + \mu n\ \nabla \Phi) + S \qquad (2.7)\\ \text{Anode}: &\quad S = \frac{jA}{F}\\ \text{Membrane}: &\quad S = 0\\ \text{Cathode}: &\quad S = -\frac{n}{n_{\text{ref}}}\frac{jA}{F}, \end{aligned}$$

where j is the total current density, A is the electrode surface area to volume ratio, F is the Faraday constant, and n_{ref} is the reference concentration taken to be 40.88 [mol/m^3] [12]. The ratio $\frac{n}{n_{\text{ref}}}$ is used for the sink term in the cathode since the total current is diminished by a decrease in concentration according to the modified Bulter-Volmer equation which relates the current through an electrode to the electric potential across the electrode. When the concentration of protons in the cathode is zero, no current flows through the cell and the cell shuts down. The concentration ratio is used to account for this effect. The ratio is assumed to be unity in the anode [1].

Table 2.3: Boundary conditions for hydrogen concentration

Left Boundary	Anode/Membrane	Membrane/Cathode	Right Boundary
$x = x_A = 0$	$x = x_{AM}$	$x = x_{MC}$	$x = x_C$
$n_A = n_0$	$n_A = n_M$	$n_M = n_C$	
	$\vec{J_A} \cdot \hat{n} = \vec{J_M} \cdot \hat{n}$	$\vec{J_M} \cdot \hat{n} = \vec{J_C} \cdot \hat{n}$	$\vec{J_C} \cdot \hat{n} = K_{MT}[n_C - n_0]$

The boundary conditions for hydrogen concentration are shown in Table 2.3. The left boundary between the anode catalyst layer and anode water channel occurs at $x = x_A$ which is taken to be zero, the boundary between the anode catalyst layer and membrane occurs at $x = x_{AM}$, the boundary between the membrane and cathode catalyst layer occurs at $x = x_{MC}$, and the right boundary between the cathode catalyst layer and cathode water channel occurs at $x = x_C$ as shown in Figure 2.1.

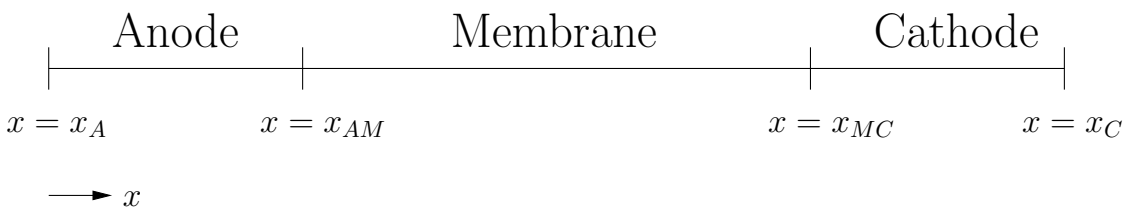

Figure 2.1: Coordinate system.

Water is pumped into the water channel which interacts with the left boundary of the model. The water is assumed to be pH 7 (neutral) which corresponds to $n_0 = 10^{-4}$ [mol/m^3]. Continuity of concentration and continuity of flux is used at each of the inner cell boundaries. On the right boundary, the cathode is actually in contact with the water channel. Since this portion of the cell is not included in the current model, the effects of the water channel must be included in the boundary conditions. Hydrogen travels through the boundary between the cathode and water channel and is then captured for fuel. The amount of hydrogen that passes through the right boundary can be characterized by the mass transfer coefficient, K_{MT}, where $\vec{J} \cdot \hat{n} = K_{MT}[n - n_0]$ and $\hat{n}$ is the unit vector normal to the boundary. Note that for $K_{MT} = 0$, the boundary condition simplifies to $\vec{J} \cdot \hat{n} = 0$ or no flux of protons through the boundary. At the other extreme, $K_{MT} = \infty$, the condition forces $n = n_0$ on the boundary.

2.1.2 Electric potential

Since the electric field must be known in order to solve the hydrogen concentration equations, the electric potential is solved throughout the PEM PEC. The flux of charge is equal to the current flowing through the cell. Using Ohm's law,

$$\begin{aligned} \vec{J} &= \vec{j} \\ &= \sigma \vec{E} \\ &= \sigma(-\nabla \Phi), \end{aligned} \tag{2.8}$$

where σ is the proton conductivity. The SO_3^- charges line the wall of the Nafion membrane and are represented in our model by delta functions [5]. An equal number of H^+ charges is present in order for the system to be electro-neutral. Due to the presence of the point charges, Gauss's law is used in the membrane since it relates the electric field to the space charge density, ρ. The charge density of an H^+ charge is equal to q/V and an SO_3^- charge is equal to $-q/V$, where V is the approximate volume between the charges in a channel of Nafion and q is the fundamental charge of a proton. Although Nafion has a very tortuous structure, the volume of the channel is taken to be 3nm $\times$ 3nm $\times$ L_M where L_M is the length of the membrane [6]. The membrane equation then becomes

$$\begin{aligned} \nabla \cdot (\epsilon \vec{E}) &= \rho \\ &= \frac{q}{V} \sum_k \left[\delta_k^{H^+} - \delta_k^{SO_3^-} \right], \end{aligned} \tag{2.9}$$

where ϵ is the permittivity of the membrane, and $\delta_k^{H^+}$ and $\delta_k^{SO_3^-}$ represent H^+ and SO_3^- charges respectively. The delta functions are assumed to be evenly distributed throughout the membrane as described in Section 2.3. The permittivity of water is assumed to be constant throughout the cell at $\epsilon = 78.0\epsilon_0$, where ϵ_0 is the vacuum permittivity [5]. The magnitude of the source term in the anode and sink term in the cathode is found by multiplying the total volume current density flowing through the cell, which is equal to the current density j [A/m^2], by the surface area/volume ratio

of the electrodes A [m^{-1}]. The complete set of electric potential equations is then

$$\begin{aligned} &\text{Anode}: && 0 = \nabla \cdot (\sigma\ \nabla\Phi) + jA \\ &\text{Membrane}: && 0 = \nabla \cdot (\epsilon\ \nabla\Phi) + \frac{q}{V}\sum_k \left[\delta_k^{H^+} - \delta_k^{SO_3^-}\right] \\ &\text{Cathode}: && 0 = \nabla \cdot (\sigma\ \nabla\Phi) - \frac{n}{n_{\text{ref}}} jA. \end{aligned} \tag{2.10}$$

Boundary conditions for electric potential are shown in Table 2.4. The total potential drop across the cell is the sum of the thermodynamic equilibrium potential V_0 and each of the overpotentials throughout the cell. An overpotential is a required potential for the reaction to occur in excess to the equilibrium potential. Each region has a corresponding overpotential, η_A for the anode, η_M for the membrane, and η_C for the cathode. The overpotential due to interface resistance, η_I, is split evenly between both interfaces (anode/membrane and membrane/cathode).

Table 2.4: Boundary conditions for electric potential

Left Boundary	Anode/Membrane	Membrane/Cathode	Right Boundary
$x = x_A = 0$	$x = x_{AM}$	$x = x_{MC}$	$x = x_C$
$\Phi_A = V_0 + \eta_A - \eta_C$ $+\eta_M + \eta_I$	$\Phi_A = \Phi_M + \frac{\eta_I}{2}$ $\epsilon_A \nabla\Phi_A \cdot \hat{n}$ $= \epsilon_M \nabla\Phi_M \cdot \hat{n}$	$\Phi_M = \Phi_C + \frac{\eta_I}{2}$ $\epsilon_M \nabla\Phi_M \cdot \hat{n}$ $= \epsilon_C \nabla\Phi_C \cdot \hat{n}$	$\Phi_C = 0$

2.1.3 Temperature

Conservation of energy is used to solve for the temperature distribution throughout the PEM PEC. According to Fourier's law of heat conduction, the energy flux is

$$\vec{J} = -\kappa \nabla T, \tag{2.11}$$

where κ is the thermal conductivity and T is the cell temperature. Each region contains a source term due to Joule heating which is caused by a current passing through a resistive material. Generated heat due to resistance is given by j^2/σ [W/m^3]. The anode also has two other source terms due to the irreversible heat produced from the electrochemical reaction and reversible entropic heat [15]. The complete set of temperature equations is then

$$\begin{aligned} 0 &= \nabla \cdot (\kappa \nabla T) + S \qquad (2.12)\\ \text{Anode}: &\quad S = \frac{j^2}{\sigma} + jA\eta_A + jA\frac{dV_0}{dT}T \\ \text{Membrane}: &\quad S = \frac{j^2}{\sigma} \\ \text{Cathode}: &\quad S = \frac{j^2}{\sigma}. \end{aligned}$$

The temperature on the outer edge of the PEM PEC is assumed to be held constant at a reference temperature, T_0. The default reference temperature is taken to be 353 K with the effects of changing the reference temperature studied in Chapter IV. As with concentration, the boundary conditions for temperature inside the cell are continuity and continuity of flux. These are summarized in Table 2.5.

Table 2.5: Boundary conditions for temperature

Left Boundary	Anode/Membrane	Membrane/Cathode	Right Boundary
$x = x_A = 0$	$x = x_{AM}$	$x = x_{MC}$	$x = x_C$
$T_A = T_0$	$T_A = T_M$	$T_M = T_C$	$T_C = T_0$
	$\kappa_A \nabla T_A \cdot \hat{n} = \kappa_M \nabla T_M \cdot \hat{n}$	$\kappa_M \nabla T_M \cdot \hat{n} = \kappa_C \nabla T_C \cdot \hat{n}$	

2.1.4 Water content

Water content has been found to perform a critical role in PEM PEC performance. The cell must be properly hydrated in order to operate; either not enough water or too much water can cause the cell to shut down. The electro-osmotic drag coefficient is a critical parameter in the water content equations which is estimated by

$$n_d = \frac{2.5}{22}\lambda \tag{2.13}$$

where λ is the water content measured by the ratio of moles of H_2O molecules to moles of SO_3^- charges, although nonlinearities exist for very low water contents, especially near $\lambda = 3$ [12, 16]. This coefficient is not a conventional drift or diffusion term and is unique to the water transport equation for electrochemical systems [16]. The water diffusion coefficient is also highly dependent on water content. A piecewise function is given by Kang [12], but since the cell is assumed to be well hydrated ($\lambda > 4$) the

expression used in our model simplifies to

$$D_w = (2.563 - .33\lambda + .0264\lambda^2 - .000671\lambda^3) \times 10^{-10} \exp\left(7.9728 - \frac{2416}{\mathrm{T}}\right). \quad (2.14)$$

At a reference temperature of 353 K, the diffusivity of water is plotted as a function of λ in Figure 2.2. The sink term in the anode is calculated using Faraday's law of

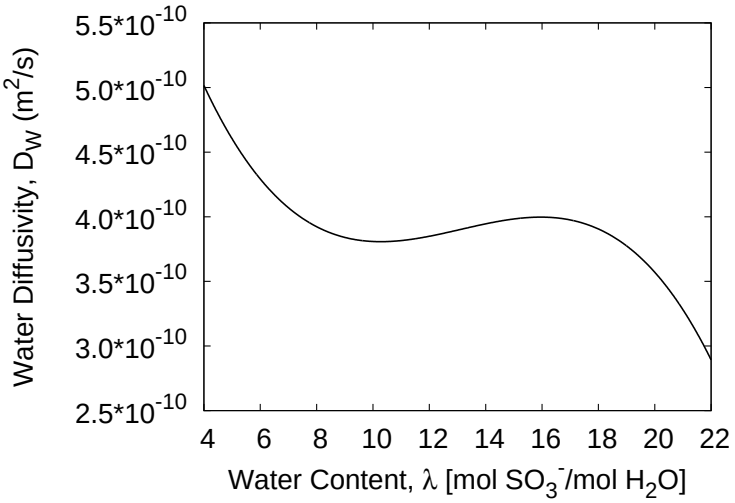

Figure 2.2: Water diffusivity as a function of λ.

electrolysis and corresponds to the water being electrolyzed into hydrogen, oxygen and electrons according to equation (1.1). Since water is neither created nor destroyed in the membrane and cathode, the source term is zero in both regions. The governing

equations for water content, as given by Kang [12], are then

$$0 = \nabla \cdot \left(\frac{\rho^{mem}}{EW} D_w \, \nabla\lambda \right) - \nabla \cdot \left(n_d \frac{j}{F} \right) + S \tag{2.15}$$

$$\text{Anode :} \qquad S = -\frac{jA}{2F}$$

$$\text{Membrane :} \quad S = 0$$

$$\text{Cathode :} \qquad S = 0,$$

where ρ^{mem} is the density of the membrane and EW is the equivalent weight of the electrolyte.

Similar to the other equations, boundary conditions for the water content are continuity of water content and continuity of diffusive flux given by $D_w \, \nabla\lambda$. Since water is pumped into both the anode and cathode water channel at a fixed rate, the outer boundaries are fixed at a reference water concentration λ_0, which is taken to be 22 [mol H_2O/mol SO_3^-]. These conditions are summarized in Table 2.6.

Table 2.6: Boundary conditions for water content

Left Boundary	Anode/Membrane	Membrane/Cathode	Right Boundary
$x = x_A = 0$	$x = x_{AM}$	$x = x_{MC}$	$x = x_C$
$\lambda_A = \lambda_0$	$\lambda_A = \lambda_M$ $D_{w_A} \nabla\lambda_A \cdot \hat{n}$ $= D_{w_M} \nabla\lambda_M \cdot \hat{n}$	$\lambda_M = \lambda_C$ $D_{w_M} \nabla\lambda_M \cdot \hat{n}$ $= D_{w_C} \nabla\lambda_C \cdot \hat{n}$	$\lambda_C = \lambda_0$

2.1.5 Other equations

The operation of the PEM PEC begins when a current density flows through the cell causing water molecules to split. The total current density through the cell is composed of an applied current density and a current density due to sunlight. While the cell acts as a solar cell, sunlight by itself does not contain enough energy to operate the cell efficiently. For this reason, a current density is applied to the cell by applying a voltage between the anode and cathode. This current density is augmented by the current density from sunlight due to the photoelectric effect, given by [4]

$$j_\nu = \frac{FI_\nu}{N_A}\frac{mc^2}{h^2\nu^2}\left(1 - \frac{\phi_{metal} + \chi}{h\nu}\right), \tag{2.16}$$

where I_ν is the intensity of light, N_A is Avagadro's constant, m is the mass of an electron, c is the speed of light, h is Planck's constant, ν is the frequency of light striking the cell, ϕ_{metal} is the work function of platinum (the catalyst coating on the electrodes), and χ is the potential difference at the electrode surface. For our model, the total current density (j) is assumed to be 1 [A/cm^2]. In effect, the current due to light decreases the required supply current density by

$$j = j_{\text{applied}} + j_\nu \qquad \Leftrightarrow \qquad j_{\text{applied}} = j - j_\nu. \tag{2.17}$$

The Butler-Volmer equation relates the current through an electrode to the electric potential across the electrode. In the anode, the equation relating the applied current density and the overpotential η_A is given by Nie [4] as

$$j_{\text{applied}} = i_A\left[\exp\left(\frac{F\eta_A}{RT}\right) - \exp\left(-\frac{F\eta_A}{RT}\right)\right], \tag{2.18}$$

where i_A is the anode exchange current density and R is the universal gas constant. In the cathode, the modified Butler-Volmer equation is used to account for the cell shutting down when no hydrogen protons reach the cathode. Without protons, no current flows and cell operation ceases. In our model, a reduced concentration of protons results in a smaller current density, hence less hydrogen production. By comparing the concentration to the reference concentration, the applied current density can be found by

$$j_{\text{applied}} = i_C \left[\frac{n}{n_{\text{ref}}} \exp\left(-\frac{F\eta_C}{RT} \right) - \frac{n}{n_{\text{ref}}} \exp\left(\frac{F\eta_C}{RT} \right) \right], \tag{2.19}$$

where i_C is the cathode exchange current density. The anode and cathode exchange current densities are temperature dependent. Using the Arrhenius equation, they can be expressed as

$$i_A = i_{A_0} \exp\left[-\frac{\mathrm{E}}{\mathrm{R}} \left(\frac{1}{\bar{\mathrm{T}}} - \frac{1}{353.15\ \mathrm{K}} \right) \right] \tag{2.20}$$

$$i_C = i_{C_0} \exp\left[-\frac{\mathrm{E}}{\mathrm{R}} \left(\frac{1}{\bar{\mathrm{T}}} - \frac{1}{353.15\ \mathrm{K}} \right) \right], \tag{2.21}$$

where i_{A_0} and i_{C_0} are the anode and cathode exchange current densities at 353.15 K, respectively, E is the activation energy, R is the universal gas constant, and $\bar{T}$ is the average temperature throughout the cell.

Solving equations (2.18) and (2.19) for η_A and η_C, the overpotential at each electrode is obtained. Overpotentials represent voltage drops in excess to the equilibrium potential required for a reaction to occur. The potential across the membrane can be found using the total current density j, conductivity of the membrane σ, and the

length of the membrane L_M. A small voltage drop also occurs at the interfaces between the regions. The total interface drop is assumed to be 5% of the equilibrium potential for water electrolysis (V_0) and is split evenly between the anode/membrane and membrane/cathode interfaces. The equations for the overpotentials and equilibrium potential are

$$\eta_A = \frac{RT}{F} \sinh^{-1}\left(\frac{j_{\text{applied}}}{2i_A}\right) \tag{2.22}$$

$$\eta_C = -\frac{RT}{F} \sinh^{-1}\left(\frac{j_{\text{applied}}}{2i_C}\frac{n_{\text{ref}}}{\overline{n}_C}\right) \tag{2.23}$$

$$\eta_M = \frac{L_M}{\sigma} j \tag{2.24}$$

$$\eta_I = .05V_0 \tag{2.25}$$

$$V_0 = 1.23 - .9 \times 10^{-3}(\bar{T} - 298.15), \tag{2.26}$$

where $\overline{n}_C$ is the average proton concentration in the cathode.

Nafion is used in the membrane because of several important properties, the most important of which is ionic conductivity. Protons must easily conduct through the membrane in order for the PEM PEC to operate. The proton conductivity of Nafion has been found to be strongly dependent on water content, given by Kang [12] as

$$\sigma = (.5139\lambda - .326) \exp\left[1268\left(\frac{1}{303} - \frac{1}{T}\right)\right]. \tag{2.27}$$

The most significant parameters in the model are the proton diffusivity and the mobility which are the driving forces that cause hydrogen protons to travel through the membrane. Intuitively, a properly hydrated membrane should have a higher diffusion coefficient than a dry membrane. By interpolating two data points, Adams

[1] finds the diffusivity to be related to the water content as

$$D = 8 \times 10^{-10}\lambda - 3.1 \times 10^{-9}. \tag{2.28}$$

Since the anode and cathode are also porous, this equation is used throughout the entire cell to describe the diffusivity. The Einstein relation can then be used to determine the mobility of protons in the cell,

$$\mu = \frac{Dq}{k_B T}, \tag{2.29}$$

where k_B is the Boltzmann constant. The relationship between water content, diffusivity, and mobility is shown in Figure 2.3.

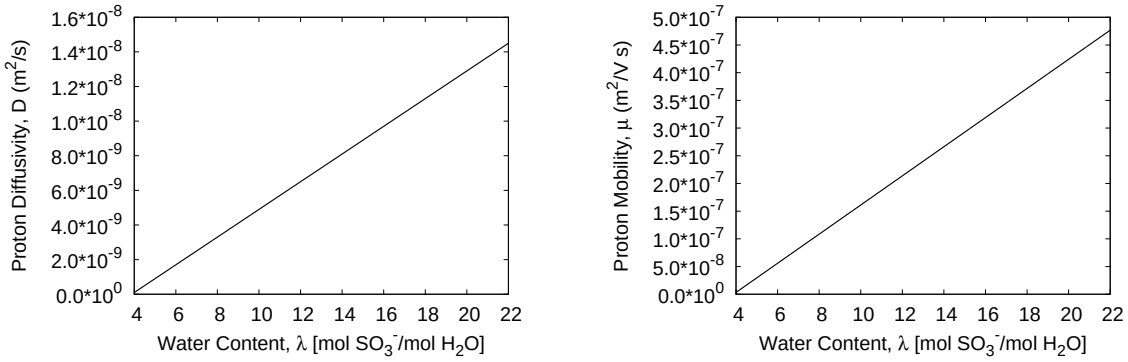

(a) Diffusivity of protons

(b) Mobility of protons

Figure 2.3: Relationship between water content, diffusivity of protons, and mobility of protons.

Once the equations are solved, the production and efficiency of the cell must be determined. Using the average proton concentration throughout the cathode ($\overline{n}_C$) in

the concentration equation sink term, the rate of hydrogen production (R_{H_2}) can be determined by

$$\begin{aligned} R_{H_2} &= \frac{\overline{n}_C}{n_{\text{ref}}} \frac{j}{F} && \left[\frac{\text{mol}}{\text{m}^2\ \text{s}}\right] \\ &= \frac{\overline{n}_C}{n_{\text{ref}}} \frac{j}{F} \frac{W_{H_2}}{\rho_{H_2}} \frac{V_C}{P + P_{\text{scaffold}}} && \left[\frac{\text{L}}{\text{s}}\right], \end{aligned} \tag{2.30}$$

where W_{H_2} is the molecular weight of hydrogen, ρ_{H_2} is the density of hydrogen, V_C is the volume of the cathode (1cm $\times$ 1cm $\times$ L_C), P is the pitch (distance between scaffolds), and P_{scaffold} is the thickness of the scaffold. For a more complete description of the pitch and other cell geometries, see Section 2.2.

Another useful quantity to characterize cell performance is the applied electrical power P_{applied}, given as

$$P_{\text{applied}} = \Phi_0 j_{\text{applied}}, \tag{2.31}$$

where Φ_0 is the electric potential at $x = 0$, given by

$$\phi_0 = V_0 + \eta_A - \eta_C + \eta_M + \eta_I. \tag{2.32}$$

Notice that the power required depends on the applied current density, so as the intensity of sunlight increases, the applied current density and the required power decrease.

2.2 Geometry

A critical aspect of cell geometry affecting hydrogen production is the structure of the nanowire assemblies composing the anode and cathode electrodes. The pitch (P)

refers to the spacing between the scaffolds and is taken to be 7μm in the default case while the thickness of the scaffold is $P_{\text{scaffold}} = 2\mu$m [7, 8, 9]. Also, a 1cm x 1cm cross-sectional area is used since the model is one-dimensional, so this structure produces the hydrogen production per cm^2. The dimensions of the cell are shown in Figure 2.4 [1].

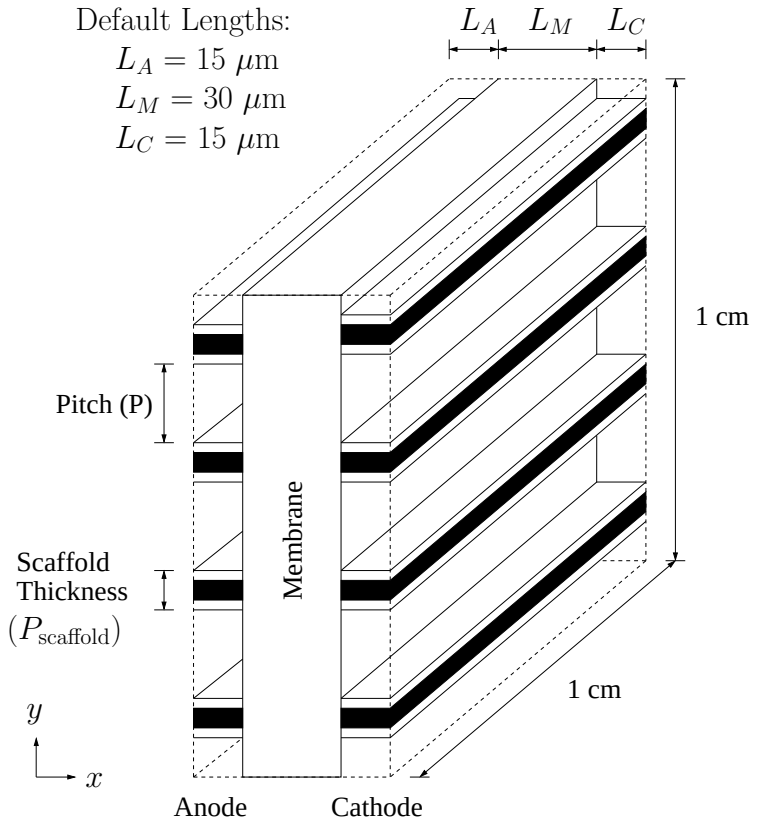

Figure 2.4: Electrode assemblies used for hydrogen production.

The PEM PEC structure is not homogenous in the y-direction since it is composed of both scaffolds and porous media between scaffolds, so this fact must be taken into account for the one-dimensional model used in this paper. Instead of using a non-homogenous structure in the y-direction, an effective area is calculated which can then be used in the one-dimensional model. Using the fact that $\vec{E} = -\nabla\Phi$, Gauss's law in two-dimensions is given by

$$\Phi_{xx} + \Phi_{yy} + \frac{\rho}{\epsilon} = 0, \tag{2.33}$$

where ρ is the charge density. To remove the dependence on y, integration is performed from the middle of a scaffold to the middle of the scaffold directly above it. The boundary condition $j = -\sigma\frac{\partial\Phi}{\partial\hat{n}}$ from Ohm's Law is used where $\hat{n}$ is a unit vector in the $\pm y$-direction depending on the direction of the electric field at the boundary ($\vec{E}$ points toward the scaffolds since they are conductors). Using the above condition and integrating over a length of $P + P_{\text{scaffold}}$ in the y-direction we find

$$\Phi_{xx} + \frac{j}{\frac{1}{2}P\sigma} + \frac{\rho}{\epsilon} = 0. \tag{2.34}$$

See Figure 2.4 for a diagram showing the pitch and orientation of the cell. For bulk water at pH 7, the charge density is electrically neutral since the space charge density of protons is equal to that of electrons, so $\rho = 0$. Comparing with equation (2.10), we find the source term is now comparable to the source term in the anode where $jA = \frac{2j}{P}$. Thus the reaction surface area of the electrode is given as

$$A = \frac{2}{P}. \tag{2.35}$$

The final equation in the anode is then

$$\sigma\Phi_{xx} + jA = 0, \tag{2.36}$$

which is the one-dimensional equivalent of equation (2.10). Thus taking $A = \frac{2}{P}$ yields a homogenized model which is independent of the y-direction. A thorough treatment of the homogenization process is given in the Appendix.

2.3 Membrane Point-Charges

The delta functions corresponding to the SO_3^- and H^+ point-charges in the membrane are assumed to be uniformly distributed. In order for the membrane to be electroneutral, the number of H^+ charges is equal to that of SO_3^- charges. The relative position of the SO_3^- and H^+ charges, *pos*, is able to vary between 0 and 0.5. When $pos = 0$, the positive and negative charges align causing the effects of the charges to cancel. For $pos = .5$, the charges are midway between opposite charges. The alignment of charges is shown in Figure 2.5. The default case of $N_{SO_3^-} = 30$ and $pos = .5$ is shown in Figure 2.6 for the entire cell.

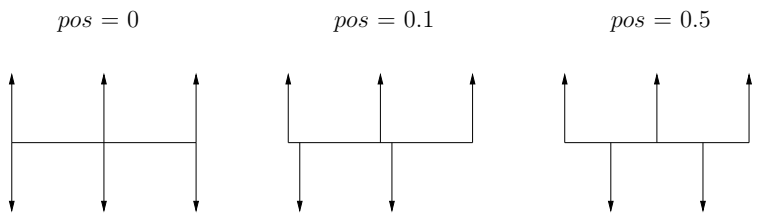

Figure 2.5: Relative position of the SO_3^- and H^+ charges.

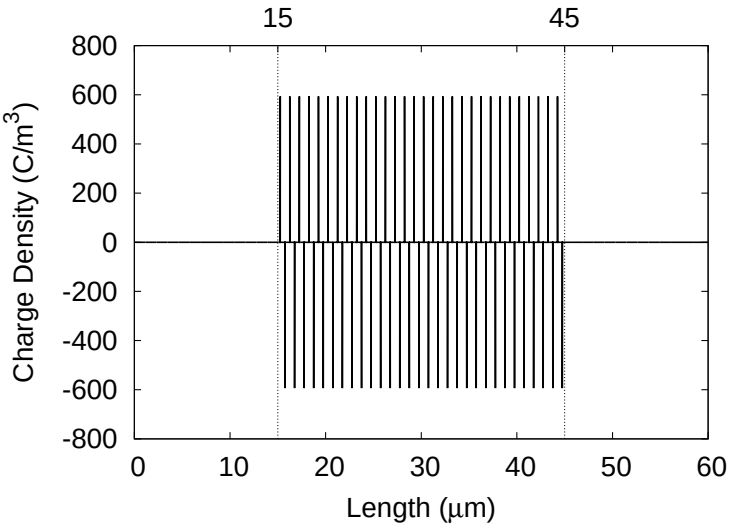

Figure 2.6: Distribution of SO_3^- and H^+ point-charges using $N_{SO_3^-} = 30$ and $pos = .5$.

2.4 Complete Model

The complete PEM PEC model consists of a set of twelve coupled PDE's. To summarize the equations that are solved in the model, Table 2.7 shows the four general governing equations while Table 2.8 lists the one-dimensional equations, Table 2.9 lists the source and sink terms applied to the governing equations in each of the three regions, and Table 2.10 lists all of the boundary conditions applied to each boundary.

Table 2.7: Governing equations

	Governing Equation
Concentration of Hydrogen	$0 = \nabla \cdot (D\ \nabla n + \mu n\ \nabla \Phi) + S$
Electric Potential (Anode/Cathode)	$0 = \nabla \cdot (\sigma\ \nabla \Phi) + S$
Electric Potential (Membrane)	$0 = \nabla \cdot (\epsilon\ \nabla \Phi) + S$
Water Content	$0 = \nabla \cdot \left(\frac{\rho^{mem}}{EW} D_w^{mem}\ \nabla \lambda\right) - \nabla \cdot \left(n_d \frac{j}{F}\right) + S$
Temperature	$0 = \nabla \cdot (\kappa\ \nabla T) + S$

Table 2.8: Governing equations (one-dimensional)

	Governing Equation
Concentration of Hydrogen	$0 = \frac{d}{dx}(D\frac{dn}{dx} + \mu n\frac{d\Phi}{dx}) + S$
Electric Potential (Anode/Cathode)	$0 = \frac{d}{dx}(\sigma\frac{d\Phi}{dx}) + S$
Electric Potential (Membrane)	$0 = \frac{d}{dx}(\epsilon\frac{d\Phi}{dx}) + S$
Water Content	$0 = \frac{d}{dx}\left(\frac{\rho^{mem}}{EW}D_w^{mem}\frac{d\lambda}{dx}\right) - \frac{d}{dx}\left(n_d\frac{j}{F}\right) + S$
Temperature	$0 = \frac{d}{dx}(\kappa\frac{dT}{dx}) + S$

Table 2.9: Source/sink terms

	Anode	**Membrane**	**Cathode**
Conc. of Hydrogen	$S = \frac{jA}{F}$	$S = 0$	$S = -\frac{n}{n_{\text{ref}}}\frac{jA}{F}$
Electric Potential	$S = jA$	$S = \frac{q}{V}\sum_k\left[\delta_k^{H^+} - \delta_k^{SO_3^-}\right]$	$S = -\frac{n}{n_{\text{ref}}}jA$
Water Content	$S = -\frac{jA}{2F}$	$S = 0$	$S = 0$
Temperature	$S = \frac{j^2}{\sigma} + jA\eta_A + jA\frac{dV_0}{dT}T$	$S = \frac{j^2}{\sigma}$	$S = \frac{j^2}{\sigma}$

Table 2.12: Universal constants

Symbol	**Description**	**Value**
c	Speed of light	2.99792458×10^{8} [m/s]
F	Faraday constant	96,485.3415 [C/mol]
h	Planck constant	$6.62606896 \times 10^{-34}$ [m^2·kg/s]
k_B	Boltzmann constant	$1.3806504 \times 10^{-23}$ [J/K]
m	Mass of an electron	$9.10938215 \times 10^{-31}$ [kg]
N_A	Avogadro constant	$6.02214179 \times 10^{23}$ [mol^{-1}]
q	Charge of a proton	$1.602176487 \times 10^{-19}$ [C]
R	Gas constant	8.314472 [J/K·mol]
ϵ_0	Vacuum permittivity	8.854187×10^{-12} [F/m]

All of the universal constants used in the paper are shown in Table 2.12. Every parameter is listed in Tables 2.13 - 2.15.

Table 2.10: Boundary conditions ($\vec{J} = D\ \nabla n - \mu n\ \nabla\Phi$)

Left Boundary	Anode/Membrane	Membrane/Cathode	Right Boundary
$x = x_A = 0$	$x = x_{AM}$	$x = x_{MC}$	$x = x_C$
$n_A = n_0$	$n_A = n_M$	$n_M = n_C$	
	$\vec{J_A} \cdot \hat{n} = \vec{J_M} \cdot \hat{n}$	$\vec{J_M} \cdot \hat{n} = \vec{J_C} \cdot \hat{n}$	$\vec{J_C} \cdot \hat{n} = K_{MT}[n_C - n_0]$
$\Phi_A = V_0 + \eta_A - \eta_C$	$\Phi_A = \Phi_M + \frac{\eta_I}{2}$	$\Phi_M = \Phi_C + \frac{\eta_I}{2}$	$\Phi_C = 0$
$+\eta_M + \eta_I$	$\epsilon_A \nabla\Phi_A \cdot \hat{n} = \epsilon_M \nabla\Phi_M \cdot \hat{n}$	$\epsilon_M \nabla\Phi_M \cdot \hat{n} = \epsilon_C \nabla\Phi_C \cdot \hat{n}$	
$T_A = T_0$	$T_A = T_M$	$T_M = T_C$	$T_C = T_0$
	$\kappa_A \nabla T_A \cdot \hat{n} = \kappa_M \nabla T_M \cdot \hat{n}$	$\kappa_M \nabla T_M \cdot \hat{n} = \kappa_C \nabla T_C \cdot \hat{n}$	
$\lambda_A = \lambda_0$	$\lambda_A = \lambda_M$	$\lambda_M = \lambda_C$	$\lambda_C = \lambda_0$
	$D_{w_A} \nabla\lambda_A \cdot \hat{n} = D_{w_M} \nabla\lambda_M \cdot \hat{n}$	$D_{w_M} \nabla\lambda_M \cdot \hat{n} = D_{w_C} \nabla\lambda_C \cdot \hat{n}$	

Table 2.11: One-Dimensional Boundary conditions ($J = D\frac{dn}{dx} + \mu\frac{d\Phi}{dx}$)

Left Boundary	Anode/Membrane	Membrane/Cathode	Right Boundary
$x = x_A = 0$	$x = x_{AM}$	$x = x_{MC}$	$x = x_C$
$n_A = n_0$	$n_A = n_M$	$n_M = n_C$	
	$J_A = J_M$	$J_M = J_C$	$J_C = K_{MT}[n_C - n_0]$
$\Phi_A = V_0 + \eta_A - \eta_C$	$\Phi_A = \Phi_M + \frac{\eta_I}{2}$	$\Phi_M = \Phi_C + \frac{\eta_I}{2}$	$\Phi_C = 0$
$+\eta_M + \eta_I$	$\epsilon_A\frac{d\Phi_A}{dx} = \epsilon_M\frac{d\Phi_M}{dx}$	$\epsilon_M\frac{d\Phi_M}{dx} = \epsilon_C\frac{d\Phi_C}{dx}$	
$T_A = T_0$	$T_A = T_M$	$T_M = T_C$	$T_C = T_0$
	$\kappa_A\frac{dT_A}{dx} = \kappa_M\frac{dT_M}{dx}$	$\kappa_M\frac{dT_M}{dx} = \kappa_C\frac{dT_C}{dx}$	
$\lambda_A = \lambda_0$	$\lambda_A = \lambda_M$	$\lambda_M = \lambda_C$	$\lambda_C = \lambda_0$
	$D_{w_A}\frac{d\lambda_A}{dx} = D_{w_M}\frac{d\lambda_M}{dx}$	$D_{w_M}\frac{d\lambda_M}{dx} = D_{w_C}\frac{d\lambda_C}{dx}$	

Table 2.13: Parameters (Part I)

Symbol	**Description**	**Value**	**Source**
A	Surface area/volume ratio	Equation (2.35) [m^{-1}]	Appendix A
D	Diffusivity of protons	Equation (2.28) [m^2/s]	Adams [1]
D_w	Diffusivity of water	Equation (2.14) [m^2/s]	Kang [12]
E	Activation energy	73,269 [J/mol]	Kang [12]
EW	Equivalent weight of electrolyte	1.1 [kg/mol]	Kang [12]
I_ν	Radiant intensity	1.0 [W/m^2]	Adams [1]
i_{A_0}	Anode exchange current density	1.0 $\times 10^{-5}$ [A/m^2]	Nie [4]
i_{C_0}	Cathode exchange current density	30.0 [A/m^2]	Nie [4]
j_ν	Current density due to sunlight	Equation (2.16) [A/m^3]	Nie [4]
j_{applied}	Applied current density	Equations (2.18)-(2.19) [A/m^3]	Nie [4]
j	Total current density	1 [A/cm^3]	Nie [4]
L_A	Length of anode	15 [μm]	(None)
L_M	Length of membrane	30 [μm]	(None)
L_C	Length of cathode	15 [μm]	(None)
$N_{SO_3^-}$	Number of SO_3^- charges	30	(None)
n_d	Electro-osmotic drag coefficient	Equation (2.13) [mol H_2O/mol SO_3^-]	Kang [12]

Table 2.14: Parameters (Part II)

Symbol	**Description**	**Value**	**Source**
n_{ref}	Reference concentration	40.88 [mol/m^3]	Kang [12]
P	Pitch	7 [μm]	Lewis [7, 8, 9]
P_{scaffold}	Pitch of the scaffold	2 [μm]	Lewis [7, 8, 9]
P_{applied}	Applied power density	Equation (2.31) [W/m^3]	(None)
pos	Position of point-charges	.5	(None)
T_0	Boundary temperature	353 [K]	Nie [4]
W_{H_2}	Mol. weight of hydrogen	1.00794 [kg/mol]	(None)
V	Vol. between charges in Nafion	3nm $\times$ 3nm $\times L_M$ [m^3]	Paddison [6]
V_C	Volume of cathode	1cm $\times$ 1cm $\times L_C$ [m^3]	(None)
V_0	Equilibrium potential	Equation (2.26) [V]	Nie [4]
η	Overpotential	Equations (2.22) - (2.25) [V]	Nie [4]
μ	Mobility of protons	Equation (2.29) [m^2/V·s]	(None)
ρ_{H_2}	Density of hydrogen	.08988 [kg/m^3]	(None)
ρ^{mem}	Density of dry membrane	1.98 $\times 10^3$ [kg/m^3]	Afshari [15]
κ_A	Thermal cond. in anode	1.0 [W/m·K]	Kang [12]
κ_M	Thermal cond. in membrane	.95 [W/m·K]	Kang [12]
κ_C	Thermal cond. in cathode	1.0 [W/m·K]	Kang [12]

Table 2.15: Parameters (Part III)

Symbol	**Description**	**Value**	**Source**
σ	Ionic conductivity	Equation (2.27) [S/m]	Kang [12]
ϵ	Permittivity	$78\epsilon_0$ [F/m]	Akinaga [5]
ν	Frequency of sunlight	6.5×10^{15} [Hz]	Nie [4]
χ	Surface potential difference	.1 [eV]	Nie [4]
ϕ_{metal}	Work function of platinum	5.5 [eV]	(None)
ϕ_0	Total cell potential	Equation (2.32) [V]	Nie [4]
λ_0	Boundary water content	22 [mol H_2O/mol SO_3^-]	(None)

CHAPTER III

MODEL DISCRETIZATION

The PEM PEC model consists of several sets of coupled partial differential equations (PDEs). Numerical techniques are used to simultaneously solve the equations until the solution converges to steady-state. This chapter shows the discretization of each PDE and its implementation in the corresponding matrix. In general, to solve the system of equations $\mathrm{A}\vec{x} = \vec{b}$, the matrix equation is given as

$$\begin{aligned} & [\mathrm{A}_1]\ x_{i-2} \\ + & [\mathrm{A}_2]\ x_{i-1} \\ + & [\mathrm{A}_3]\ x_i \quad = \ b_i \\ + & [\mathrm{A}_4]\ x_{i+1} \\ + & [\mathrm{A}_5]\ x_{i+2}, \end{aligned} \tag{3.1}$$

along with boundary conditions

$$\begin{aligned} & [\mathrm{BC}_1]\ x_{i-2} \\ + & [\mathrm{BC}_2]\ x_{i-1} \\ + & [\mathrm{BC}_3]\ x_i \quad = \ b_i \\ + & [\mathrm{BC}_4]\ x_{i+1} \\ + & [\mathrm{BC}_5]\ x_{i+2}, \end{aligned} \tag{3.2}$$

which are implemented in the matrix as

$$\begin{bmatrix}
\mathrm{BC}_3 & \mathrm{BC}_4 & \mathrm{BC}_5 & & & & & & & & & & & & \\
\mathrm{A}_2 & \mathrm{A}_3 & \mathrm{A}_4 & \mathrm{A}_5 & & & & & & & & & & & \\
\mathrm{A}_1 & \mathrm{A}_2 & \mathrm{A}_3 & \mathrm{A}_4 & \mathrm{A}_5 & & & & & & & & & & \\
 & \mathrm{A}_1 & \mathrm{A}_2 & \mathrm{A}_3 & \mathrm{A}_4 & \mathrm{A}_5 & & & & & 0 & & & & \\
 & & \ddots & \ddots & \ddots & \ddots & \ddots & & & & & & & & \\
 & & & \mathrm{A}_1 & \mathrm{A}_2 & \mathrm{A}_3 & \mathrm{A}_4 & \mathrm{A}_5 & & & & & & & \\
 & & & & \mathrm{BC}_1 & \mathrm{BC}_2 & \mathrm{BC}_3 & \mathrm{BC}_4 & \mathrm{BC}_5 & & & & & & \\
 & & & & & \mathrm{A}_1 & \mathrm{A}_2 & \mathrm{A}_3 & \mathrm{A}_4 & \mathrm{A}_5 & & & & & \\
 & & & & & & \ddots & \ddots & \ddots & \ddots & \ddots & & & & \\
 & & & & & & & \mathrm{A}_1 & \mathrm{A}_2 & \mathrm{A}_3 & \mathrm{A}_4 & \mathrm{A}_5 & & & \\
 & & & & & & & & \mathrm{BC}_1 & \mathrm{BC}_2 & \mathrm{BC}_3 & \mathrm{BC}_4 & \mathrm{BC}_5 & & \\
 & & & 0 & & & & & & \mathrm{A}_1 & \mathrm{A}_2 & \mathrm{A}_3 & \mathrm{A}_4 & \mathrm{A}_5 & \\
 & & & & & & & & & & \ddots & \ddots & \ddots & \ddots & \ddots \\
 & & & & & & & & & & & \mathrm{A}_1 & \mathrm{A}_2 & \mathrm{A}_3 & \mathrm{A}_4 \\
 & & & & & & & & & & & & \mathrm{BC}_1 & \mathrm{BC}_2 & \mathrm{BC}_3
\end{bmatrix}
\begin{bmatrix} x_1 \\ x_2 \\ x_3 \\ x_4 \\ \vdots \\ x_{A-1} \\ x_A \\ x_{A+1} \\ \vdots \\ x_{M-1} \\ x_M \\ x_{M+1} \\ \vdots \\ x_{C-1} \\ x_C \end{bmatrix}
=
\begin{bmatrix} b_1 \\ b_2 \\ b_3 \\ b_4 \\ \vdots \\ b_{A-1} \\ b_A \\ b_{A+1} \\ \vdots \\ b_{M-1} \\ b_M \\ b_{M+1} \\ \vdots \\ b_{C-1} \\ b_C \end{bmatrix}. \tag{3.3}$$

3.1 Hydrogen Concentration

3.1.1 Governing Equation

In order for the solution to converge, the hydrogen concentration equations are solved using the Crank-Nicholson method, which takes an average of subsequent time steps. This requires the time derivative to be placed back in the equation according to equation (2.1). Convergence to the steady-state solution is then obtained by using a relatively large time step of 1ms. With the time derivative, equation (2.7) becomes

$$n_t = \nabla \cdot (D\ \nabla n + \mu n\ \nabla \Phi) + S. \tag{3.4}$$

In one-dimension,

$$\begin{aligned} n_t &= (Dn_x + \mu n \Phi_x)_x + S \\ &= Dn_{xx} + D_x n_x + \mu n \Phi_{xx} + \mu n_x \Phi_x + \mu_x n \Phi_x + S. \end{aligned} \tag{3.5}$$

Using central differences, we find the discretization equation is as follows, where k represents the position in time and i is the position in space,

$$\begin{aligned} \frac{1}{\Delta t}[n_i^{k+1} - n_i^k] = &\frac{D_i}{2\Delta x^2}[(n_{i-1}^k - 2n_i^k + n_{i-1}^k) + (n_{i-1}^{k+1} - 2n_i^{k+1} + n_{i-1}^{k+1})] \\ &+ \frac{1}{8\Delta x^2}[D_{i+1} - D_{i-1}][(n_{i+1}^k - n_{i-1}^k) + (n_{i+1}^{k+1} - n_{i-1}^{k+1})] \\ &+ \frac{\mu_i}{2\Delta x^2}[n_i^{k+1} - n_i^k][\Phi_{i-1} - 2\Phi_i + \Phi_{i+1}] \\ &+ \frac{\mu_i}{8\Delta x^2}[(n_{i+1}^k - n_{i-1}^k) + (n_{i+1}^{k+1} - n_{i-1}^{k+1})][\Phi_{i+1} - \Phi_{i-1}] \\ &+ \frac{1}{8\Delta x^2}[\mu_{i+1} - \mu_{i-1}][n_i^{k+1} - n_i^k][\Phi_{i+1} - \Phi_{i-1}] \\ &+ S_i^k. \end{aligned} \tag{3.6}$$

For simplicity, let $\tilde{r} = \Delta t/\Delta x^2$. Rearranging terms yields the matrix equation as

$$\begin{aligned}
&\left[-\frac{\tilde{r}}{2}D_i + \frac{\tilde{r}}{8}(D_{i+1} + D_{i-1}) + \frac{\tilde{r}}{8}\mu_i(\Phi_{i+1} - \Phi_{i-1})\right] n_{i-1}^{k+1} \\
&+ \left[1 + \tilde{r}D_i - \frac{\tilde{r}}{2}\mu_i(\Phi_{i+1} - 2\Phi_i + \Phi_{i-1}) - \frac{\tilde{r}}{8}(\mu_{i+1} - \mu_{i-1})(\Phi_{i+1} - \Phi_{i-1})\right] n_i^{k+1} \\
&+ \left[-\frac{\tilde{r}}{2}D_i - \frac{\tilde{r}}{8}(D_{i+1} - D_{i-1}) - \frac{\tilde{r}}{8}\mu_i(\Phi_{i+1} - \Phi_{i-1})\right] n_{i+1}^{k+1}
\end{aligned}$$

$$\begin{aligned}
&= n_i^k + \frac{\tilde{r}}{2}D_i(n_{i-1}^k - 2n_i^k + n_{i-1}^k) + \frac{\tilde{r}}{8}(D_{i+1} - D_{i-1})(n_{i+1}^k - n_{i-1}^k) \\
&\quad + \frac{\tilde{r}}{2}\mu_i n_i^k(\Phi_{i-1} - 2\Phi_i + \Phi_{i+1}) + \frac{\tilde{r}}{8}\mu_i(\Phi_{i+1} - \Phi_{i-1})(n_{i+1}^k - n_{i-1}^k) \\
&\quad - \frac{\tilde{r}}{8}n_i^k(\mu_{i+1} - \mu_{i-1})(\Phi_{i+1} - \Phi_{i-1}) + \Delta t\ S_i^k. \qquad (3.7)
\end{aligned}$$

3.1.2 Boundary Conditions

Boundary conditions for proton concentration are shown in Table 2.3. The inner boundaries are chosen to occur on a grid point in the mesh as shown in Figure 3.1. Therefore, continuity is automatically achieved since $n_1 \equiv n_2$ on the boundaries. The

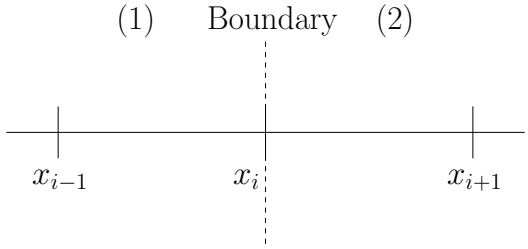

Figure 3.1: Gridpoint system used at a general boundary between materials (1) and (2) with the boundary occuring on a gridpoint.

flux boundary condition is implemented on the boundary between materials (1) and (2) by

$$D_1 \frac{dn_1}{dx} + \mu_1 n_1 \frac{d\Phi_1}{dx} = D_2 \frac{dn_2}{dx} + \mu_2 n_2 \frac{d\Phi_2}{dx}. \tag{3.8}$$

Letting x_i be the point on the boundary and using second-order forward and backward differences, we find the discretized equation is

$$\begin{aligned} &\frac{D_1}{2\Delta x}\left[n_{i-2} - 4n_{i-1} + 3n_i\right] + \frac{\mu_1 n_i}{2\Delta x}\left[\Phi_{i-2} - 4\Phi_{i-1} + 3\Phi_i\right] \\ &\qquad = \frac{D_2}{2\Delta x}\left[-3n_i + 4n_{i+1} - n_{i+2}\right] + \frac{\mu_2 n_i}{2\Delta x}\left[-3\Phi_i + 4\Phi_{i+1} - \Phi_{i+2}\right]. \end{aligned} \tag{3.9}$$

Since the second-order boundary conditions are used, the matrix structure must be pentadiagonal. The continuity of flux is implemented in the matrix as

$$\begin{aligned} & & & & & & [D_1]\ n_{i-2} & & \\ & & & & & + [-4D_1]\ n_{i-1} & & & \\ + [3(D_1+D_2) + \mu_1(\Phi_{i-2} - 4\Phi_{i-1} + 3\Phi_i) - \mu_2(-3\Phi_i + 4\Phi_{i+1} - \Phi_{i+2})]\ n_i & & & = & & 0 & & \\ & & & & & + [-4D_2]\ n_{i+1} & & & \\ & & & & & + [D_2]\ n_{i+2}. & & & \end{aligned} \tag{3.10}$$

The boundary condition for the right boundary is obtained in a similar manner and is implemented as

$$\begin{aligned} & [D_i]\ n_{i-2} \\ & + [-4D_i]\ n_{i-1} \\ + [3D_i + \mu_i(\Phi_{i-2} - 4\Phi_{i-1} + 3\Phi_i) - 2K_{MT}\Delta x]\ n_i \quad &= \ -2K_{MT} n_0 \Delta x \\ & + [-4D_2]\ n_{i+1} \\ & + [D_2]\ n_{i+2}, \end{aligned} \tag{3.11}$$

where i is the gridpoint on the right boundary.

3.2 Electric Potential

3.2.1 Governing Equation

The governing equation for electric potential in the anode and cathode is given as

$$\begin{aligned} 0 &= \nabla \cdot (\sigma \nabla \Phi) + S \\ &= \sigma \nabla^2 \Phi + \nabla \sigma\ \nabla \Phi + S. \end{aligned} \tag{3.12}$$

In one-dimension, we have

$$0 = \sigma \Phi_{xx} + \sigma_x \Phi_x + S. \tag{3.13}$$

The electrical conductivity, σ, is both water and temperature dependent (so also spatially dependent) and is discretized using central differences along with the electric potential, Φ, as

$$0 = \frac{\sigma}{\Delta x^2} \left[\Phi_{i-1} - 2\Phi_i + \Phi_{i+1}\right] + \frac{1}{4\Delta x^2} \left[\sigma_{i+1} - \sigma_{i-1}\right] \left[\Phi_{i+1} - \Phi_{i-1}\right] + S. \tag{3.14}$$

In order to increase the speed of the solution, the matrix is kept constant and only the right-hand-side is changed. For this reason, the matrix is setup as

$$\begin{aligned} [1]\ \Phi_{i-1} & \\ +\ [-2]\ \Phi_i \quad &= \ -\frac{\Delta x^2}{\sigma_i}\ S - \frac{1}{4\sigma_i}(\sigma_{i+1} - \sigma_{i-1})(\Phi_{i+1} - \Phi_{i-1}) \\ +\ [1]\ \Phi_{i+1}. & \end{aligned} \tag{3.15}$$

3.2.2 Boundary Conditions

Boundary conditions for electric potential are given in Table 2.4. Since the boundary exists on a grid point, the interface resistance overpotential cannot be accounted for in the matrix. To simplify the implementation, the appropriate interface potential is simply added to each region once steady-state has been reached. For this reason, the η_I term is removed from the left boundary condition during implementation. The general continuity of flux boundary condition between materials (1) and (2) in one-dimension is given by

$$\epsilon_1 \frac{d\Phi_1}{dx} = \epsilon_2 \frac{d\Phi_2}{dx}. \tag{3.16}$$

Discretizing the equation using second-order forward and backward central differences, we find

$$\frac{\epsilon_1}{2\Delta x}\left[\Phi_{i-2} - 4\Phi_{i-1} + 3\Phi_i\right] = \frac{\epsilon_2}{2\Delta x}\left[-3\Phi_i + 4\Phi_{i+1} - \Phi_{i+2}\right]. \tag{3.17}$$

Rearranging the equation, the boundary conditions are implemented in the matrix as

$$\begin{aligned} & [\epsilon_1]\ \Phi_{i-2} \\ + & [-4\epsilon_1]\ \Phi_{i-1} \\ + & [3(\epsilon_1+\epsilon_2)]\ \Phi_i \quad = \ 0 \\ + & [-4\epsilon_2]\ \Phi_{i+1} \\ + & [\epsilon_1]\ \Phi_{i+2}. \end{aligned} \tag{3.18}$$

3.3 Temperature

3.3.1 Governing Equation

The thermal conductivity is material dependent and is therefore taken to be constant throughout each region. Using this assumption, we find equation (2.12) becomes

$$0 = \kappa\ \nabla^2 T + S. \tag{3.19}$$

Using a finite difference approximation for the one-dimensional model, we have

$$0 = \frac{\kappa}{\Delta x^2}\left[T_{i-1} - 2T_i + T_{i+1}\right] + S. \tag{3.20}$$

This equation is implemented in the matrix as

$$\begin{aligned} & [\kappa]\ T_{i-1} \\ + & [-2\kappa]\ T_i \quad = \ -\Delta x^2\ S \\ + & [\kappa]\ T_{i+1}. \end{aligned} \tag{3.21}$$

3.3.2 Boundary Conditions

Continuity of temperature is automatically achieved by use of the one-point boundary since $T_1 \equiv T_2$. Continuity of flux between materials (1) and (2) is given by

$$\kappa_1 \frac{dT_1}{dx} = \kappa_2 \frac{dT_2}{dx}. \tag{3.22}$$

Discretizing the equation with second-order forward and backward differences, we find

$$\frac{\kappa_1}{2\Delta x^2}\left[T_{i-2} - 4T_{i-1} + 3T_i\right] = \frac{\kappa_2}{2\Delta x^2}\left[-3T_i + 4T_{i+1} - T_{i+2}\right]. \tag{3.23}$$

This yields the matrix equation

$$\begin{aligned}
&[\kappa_1]\ T_{i-2} \\
+\ &[-4\kappa_1]\ T_{i-1} \\
+\ &[3(\kappa_1 + \kappa_2)]\ T_i \quad = \ 0 \\
+\ &[-4\kappa_2]\ T_{i+1} \\
+\ &[\kappa_2]\ T_{i+2}.
\end{aligned} \tag{3.24}$$

3.4 Water Content

3.4.1 Governing Equation

The governing equation for water content is given by equation (2.15). The product rule is used for the diffusivity of water since the parameter is highly dependent on water content. Using second-order central differences, we find the discretized equation

is

$$
\begin{aligned}
0 = & \frac{\rho^{mem}}{EW}\frac{D_{w_i}}{\Delta x^2}\left[\lambda_{i-1} - 2\lambda_i + \lambda_{i+1}\right] \\
& + \frac{\rho^{mem}}{EW}\frac{1}{4\Delta x^2}\left[D_{w_{i+1}} - D_{w_{i-1}}\right]\left[\lambda_{i+1} - \lambda_{i-1}\right] \\
& - \frac{2.5}{22}\frac{i}{F}\frac{1}{2\Delta x}\left[\lambda_{i+1} - \lambda_{i-1}\right]. \qquad (3.25)
\end{aligned}
$$

This yields the matrix equation,

$$
\begin{aligned}
\left[\frac{\rho^{mem}}{EW}\left(D_{w_i} - \frac{D_{w_{i+1}} - D_{w_{i-1}}}{4}\right) + \Delta x\frac{2.5}{22}\frac{i}{F}\right]\lambda_{i-1} & \\
+ \left[-2\frac{\rho^{mem}}{EW}D_{w_i}\right]\lambda_i \quad &= -\Delta x^2\ S \\
+ \left[\frac{\rho^{mem}}{EW}\left(D_{w_i} + \frac{D_{w_{i+1}} - D_{w_{i-1}}}{4}\right) - \Delta x\frac{2.5}{22}\frac{i}{F}\right]\lambda_{i+1}. & \qquad (3.26)
\end{aligned}
$$

3.4.2 Boundary Conditions

Continuity of water content between regions is automatically achieved by use of the one-point boundary. Therefore, the continuity of flux condition is applied on the boundary. For a boundary between materials (1) and (2), the equation is

$$
D_{w_1}\frac{d\lambda_1}{dx} = D_{w_2}\frac{d\lambda_2}{dx}, \qquad (3.27)
$$

which can be discretized using second-order forward and backward differences as

$$
\frac{D_{w_1}}{4\ \Delta x}\left[\lambda_{i-2} - 4\lambda_{i-1} + 3\lambda_i\right] = \frac{D_{w_2}}{4\ \Delta x}\left[-3\lambda_i + 4\lambda_i - \lambda_{i+2}\right]. \qquad (3.28)
$$

Arranging the equation, we find the matrix equation

$$\begin{aligned}
&[D_{w_1}]\ \lambda_{i-2} \\
&+ [-4D_{w_1}]\ \lambda_{i-1} \\
&+ [3(D_{w_1} + D_{w_2})]\ \lambda_i \quad = \ 0 \\
&+ [-4D_{w_2}]\ \lambda_{i+1} \\
&+ [D_{w_2}]\ \lambda_{i+2}.
\end{aligned} \tag{3.29}$$

CHAPTER IV

RESULTS AND DISCUSSION

In this chapter, the results are shown for several different sets of cell parameters to analyze the effects of each parameter. By doing so, we aim to identify characteristics of the cell which can be modified to produce a more efficient hydrogen-producing mechanism. Since hydrogen is the most important output of the cell while supplied power is the main input, both will be studied for each test case. In order to have a basis for comparison, a default case is first studied, and then all future results are compared to the default case. The parameters used in the default case are shown in Table 4.1.

The hydrogen production and input power for each of the following cases are listed in Tables 4.2 and 4.3 for reference. The default case produces about 6 [ml/min] of hydrogen gas to be used for fuel. As can be seen from the tables, cell parameters can have a significant effect on the amount of hydrogen production which ranges from under 2 to over 22 [ml/min]. These variations must be taken advantage of in order to produce an economical and efficient PEM PEC for hydrogen production. Solving the governing equations for proton concentration, electric potential, temperature, and water content throughout the anode, membrane, and cathode of the PEM PEC for the default case yields the results shown in Figure 4.1. Note that the vertical dashed

Table 4.1: Default parameters

Description	**Symbol**	**Value**
Reference Temperature	T_0	353 [K]
Number of SO_3^- groups	$N_{SO_3^-}$	30
Position of SO_3^- groups	pos	0.5
Water content	λ_0	22 [mol SO_3^-/mol H_2O]
Light source intensity	I_ν	0.1 [mW/cm^2]
Pitch	P	7 [μm]
Length of Anode	L_A	15 [μm]
Length of Membrane	L_M	30 [μm]
Length of Cathode	L_C	15 [μm]
Mass transfer coefficient	K_{MT}	.01

lines in all plots refer to the boundaries of the cell, separating the results into each of the three regions. It should also be noted that each of the plots refers to the steady-state conditions of the cell since steady-state was assumed in the forming of the governing equations. Steady-state is considered to be reached when the L_2 norm of the proton concentration is less than a tolerance of 10^{-3}.

The proton concentration profile in Figure 4.1(a) reveals the distribution of protons in the cell at steady-state. As the water pumped into the cell at the anode (left) is

Table 4.2: Hydrogen production (Part I)

Test Case	**H_2 Production**		**Power [W/cm^2]**
	[ml/min]	**% of Default**	
Default	5.8589	100.0 %	2.0476
T = 333 K	5.7983	99.0 %	2.1028
T = 303 K	5.9680	101.9 %	2.1844
100 SO_3^- and H^+ Charges	5.8766	100.3 %	2.0475
300 SO_3^- and H^+ Charges	5.9272	101.2 %	2.0473
pos = .25	5.9096	100.9 %	2.0474
pos = .1	5.9392	101.4 %	2.0472
$\lambda_0 = 8$	12.7318	217.3 %	2.0240
$\lambda_0 = 6$	0.0690	1.2 %	2.2000
Half Mobility	7.5247	128.4 %	2.0400
No Mobility	1.6417	28.0 %	2.0863
$I_\nu = 0.6$ mW/cm^2	5.8923	100.6 %	2.0261
$I_\nu = 1.2$ mW/cm^2	5.9600	101.7 %	1.9829

electrolyzed, the concentration of protons increases from that of neutral water (pH 7). The protons travel through the channels of Nafion in the membrane (middle) until they reach the cathode (right) where the protons are removed from the system

Table 4.3: Hydrogen production (Part II)

Test Case	**H_2 Production**		**Power [W/cm^2]**
	[ml/min]	**% of Default**	
Default	5.8589	100.0 %	2.0476
$P = 5\mu m$	9.5327	162.7 %	2.0404
$P = 3\mu m$	17.9140	305.8 %	2.0312
$K_{MT} = 0$	12.2049	208.3 %	2.0253
$K_{MT} = \infty$	5.4657	93.3 %	2.0498
$L_A = L_C = 10\mu m$	2.4263	41.4 %	2.0690
$L_A = L_C = 30\mu m$	22.5323	384.6 %	2.0184
$L_M = 20\mu m$	5.2720	90.0 %	2.0453
$L_M = 40\mu m$	6.3376	108.2 %	2.0499

to be stored for fuel. The mass transfer coefficient describes the rate at which the protons transfer from the cathode to the water channel. Since the protons are not immediately swept away by the water channel, a small pile-up of protons occurs on the right boundary of the cell. The amount of hydrogen produced corresponds to the sink term in the cathode, so a large concentration throughout the cathode is desired to increase hydrogen production.

While the proton concentration plot corresponds to the output of the cell, the electric

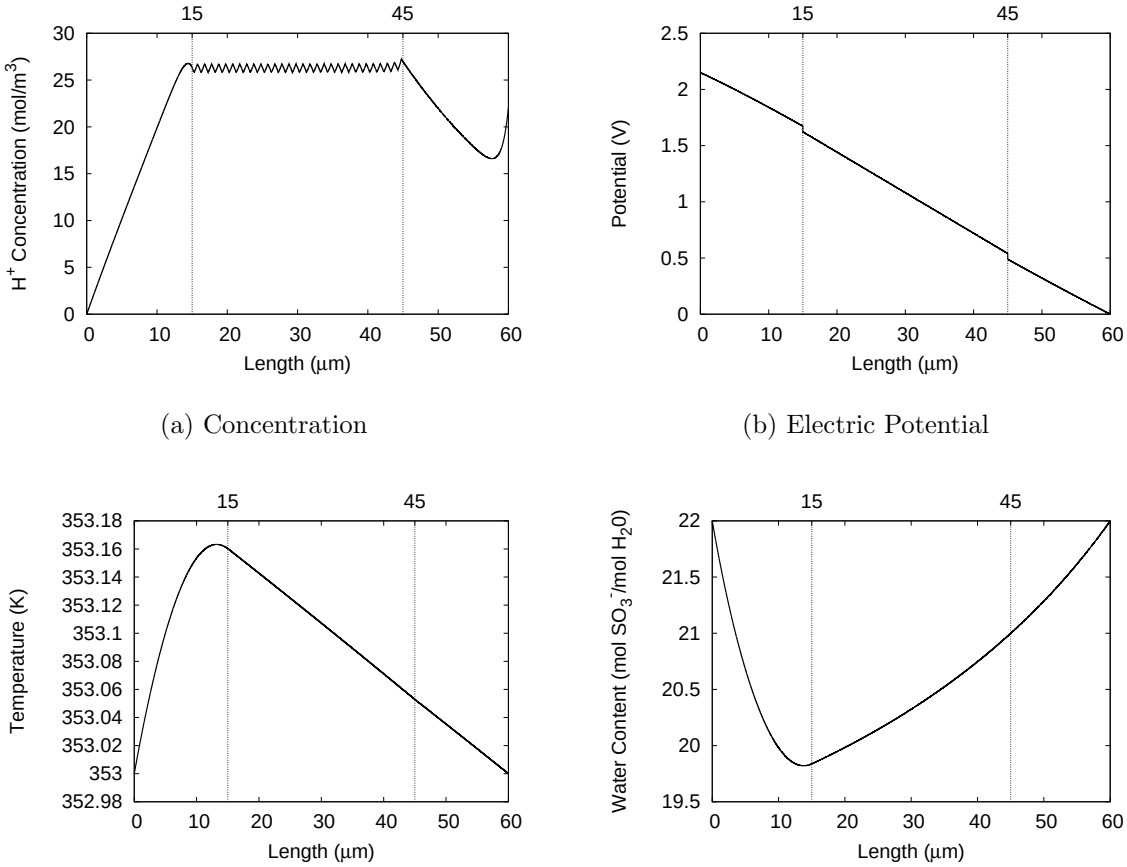

(a) Concentration

(b) Electric Potential

(c) Temperature

(d) Water Content

Figure 4.1: Default plots for the PEM PEC.

potential plot shown in Figure 4.1(b) corresponds to the input of the cell. Since the applied current density is assumed to be constant, the required power density given by equation (2.31) is proportional to the applied cell voltage, Φ_0. Thus it is desired to have the electric potential at the left boundary as low as possible to decrease the required power. The shape of the plot is nearly linear, except for the small discontinuities at the boundaries due to interface resistance. The linear shape is

expected since a relative permittivity of 78.0 is used in each region due to the porous nature of the cell. The discontinuities at the boundaries arise from the imposed condition of a $.05V_0$ potential drop due to interface resistance.

The temperature in the cell increases slightly in the anode due to the heat produced from the electrolysis of water as seen in Figure 4.1(c). Joule heating caused by passing a current through a material is also taken into account, but has little effect in the other regions of the cell. It should be noted that Kang [12] reports a temperature difference of about 5 °C throughout the cell. This difference, however, is due to the inclusion of the gas diffusion layers in the model which are several orders of magnitude longer than the anode, membrane, and cathode regions. The temperature increase in these regions of the model used by Kang is of the same order as our model.

The water content throughout the cell, shown in Figure 4.1(d), must be monitored so that the cell does not become saturated or dry, either of which will cause it to shut down. The water content decreases in the anode as water is electrolyzed into hydrogen, oxygen, and electrons. Water is pumped into the cell at $\lambda_0 = 22$ at both the anode and cathode in order to maintain proper hydration levels throughout the cell.

4.1 Effects of Temperature

In practical applications, photoelectrochemical cells must be able to operate in various conditions including low temperatures. Although many of the parameters are temperature dependent, the main effects of a decrease in temperature are on the elec-

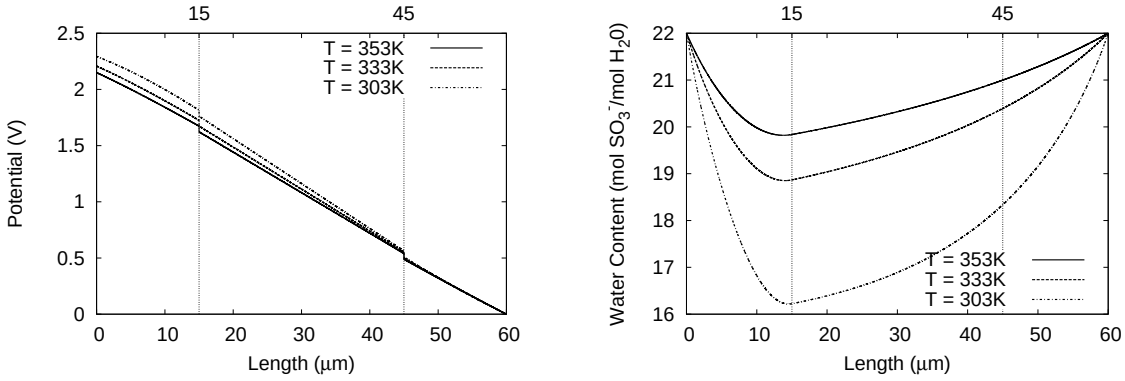

(a) Electric Potential

(b) Water Content

Figure 4.2: Electric potential and water content profiles for low temperature conditions.

tric potential and water content profiles as seen in Figure 4.2. The applied potential is composed of the equilibrium potential and all of the overpotentials throughout the cell. As temperature decreases, the anode and cathode overpotentials increase along with the equilibrium potential of the electrolysis reaction. This causes the applied potential to increase, requiring more input power for the cell to operate. These results are consistent with those of Nie [4]. The water content is strongly dependent on the diffusivity of water which is a function of temperature. Decreasing the temperature also decreases the diffusivity of water, causing less water to flow through the cell. If the temperature becomes too low, the cell will become dry and cease to operate. In both cases, the cell should operate in a high temperature environment. Higher temperatures require less input power and inhibit the cell from becoming dry.

It should be noted that Nie [4] found an 11% increase in hydrogen production from

303K to 353K. In our model, the effects of temperature have been shown to be less significant, resulting in only a 1.9% increase in hydrogen production over the given temperature range. Both models are consistent, however, in that higher temperatures result in greater hydrogen production rates.

4.2 Effects of Charges in Membrane

The presence of SO_3^- charges in the Nafion membrane is used to provide a hopping mechanism to move protons through the membrane more efficiently [5]. One of the

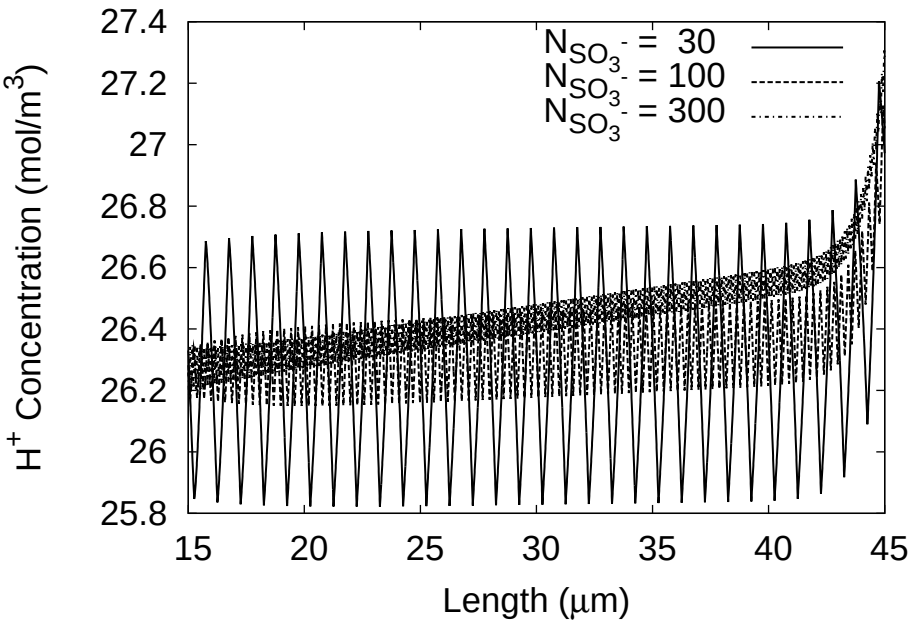

Figure 4.3: Concentration profile in the membrane for $N_{SO_3^-}$ = 30, 100, and 300 charges.

main features of this model is the incorporation of the SO_3^- charges as delta functions. By doing so, the model can quantify the effectiveness of the charges in the membrane along with determining the effects of the number and position of the charges. Figure 4.3 shows the proton concentration profile in the membrane for different numbers of charges. While the lower number of charges produces higher concentration swings, the average value is lower than when more charges are used. The difference between average proton concentrations for 30 and 100 charges is small compared to that of 300 charges. Hydrogen production increased very little when the number of charges increased to 100, and increased by .07 [ml/min] over the default case for 300 charges.

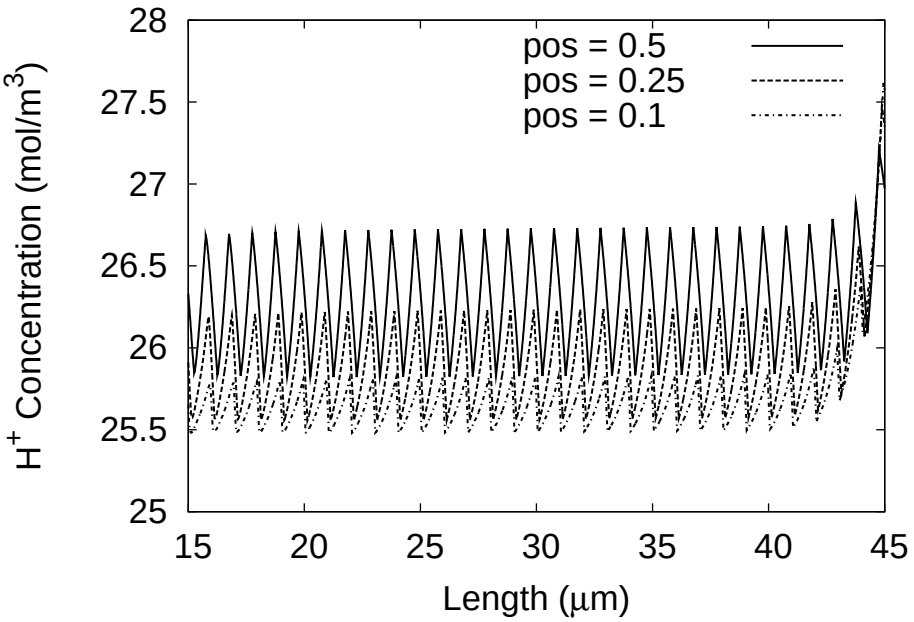

Figure 4.4: Concentration profile in the membrane for SO_3^- spacing pos = 0.5, 0.25, and 0.1.

Physical limitations limit the number of SO_3^- charges that can be placed in the membrane. The closest the charges can be is about 1nm which corresponds to 1,000 charges. Also, it should be noted that as more charges are introduced into the membrane, the charges cancel out more since they are closer together. This effect is shown in Figure 4.4. As the spacing between charges is decreased, the proton concentration decreases. Thus using too many charges can result in a decrease in hydrogen production, although using more charges increases the hydrogen output to a certain point. This is a delicate balancing act, although the overall increase in hydrogen production is small compared to the effects of other parameters.

4.3 Effects of Water Content

The PEM PEC must be properly hydrated in order to produce hydrogen. Water content affects many parameters in the model including proton diffusivity, proton conductivity, proton mobility, and water diffusivity. Figure 4.5 shows the proton distribution for several values of water content. In the extreme cases of either complete saturation or dehydration, hydrogen production ceases leaving the cell inoperational. As water content increases, the mobility of protons also increases as shown by equations 2.28 and 2.29. The increase in mobility allows more protons to flow through the membrane to the cathode, but this is counteracted by the increase in diffusivity which causes the proton distribution to flatten out across the entire cell. The overall effect is a slight decrease in hydrogen production as shown in Figure 4.6. A distinct feature of the plot reveals that hydrogen production suddenly decreases drastically

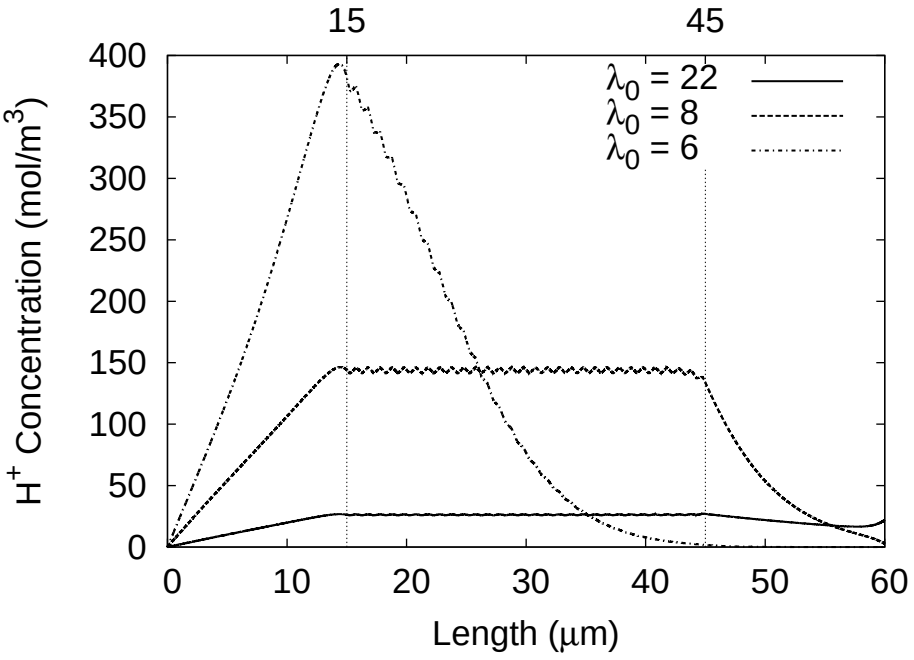

Figure 4.5: Concentration profile for boundary water contents of $\lambda_0 = 22$, 8, and 6.

at a water content of $\lambda_0 = 6.3$ [mol H_2O/mol SO_3^-]. The reason for this can be seen from Figure 4.5. At very low water contents, the mobility of protons is also very low which prohibits the protons from passing through the membrane to the cathode. A large pile-up occurs at the anode/membrane interface, but very little hydrogen is produced since very few protons reach the cathode. This situation corresponds to the cell over-heating and becoming dehydrated which must be avoided during operation. For efficient cell operation, hydrogen production can be more than doubled by lowering the water content to $\lambda = 8$ [mol H_2O/mol SO_3^-], although caution must be used to keep the cell from becoming dehydrated and inoperational.

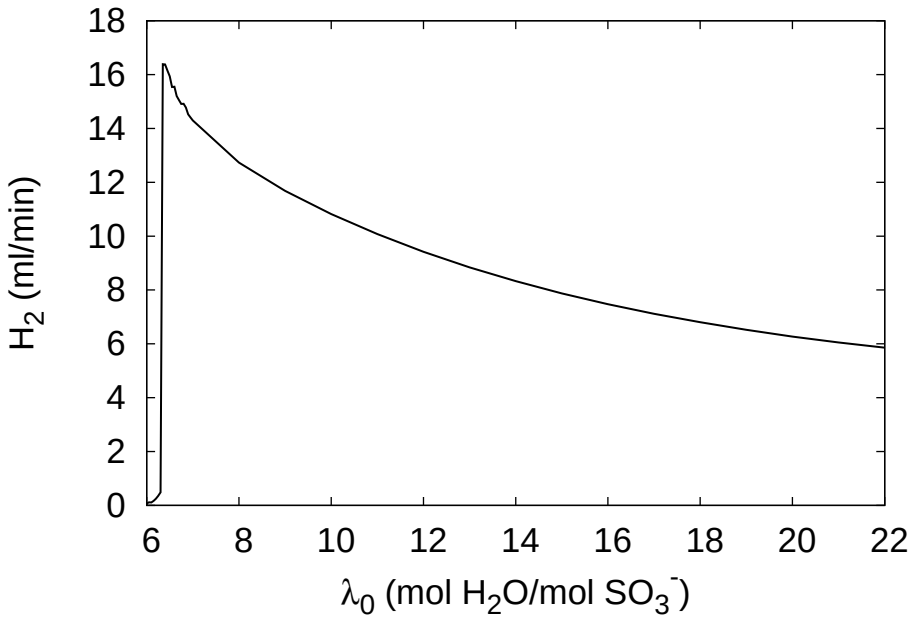

Figure 4.6: Hydrogen production as a function of water content.

4.4 Effects of Mobility

Mobility plays a critical role in transporting protons through the Nafion membrane. Without the effects of mobility, diffusion is the only source of proton transport and the amount of hydrogen production decreases severely. Figure 4.7 shows the proton concentration throughout the cell for full, half, and no mobility scenarios with the mobility calculated according to equation 2.29 and then multiplied by 1, 0.5, and 0 respectively. As the mobility of protons is decreased, protons pile up in the anode as electrolysis continues to occur, but the protons do not get carried through the membrane. Few protons reach the cathode resulting in very low hydrogen output. For this reason, it is critical that mobility not be impaired in the PEM PEC. It

is interesting to note, however, that hydrogen production actually increased for the half mobility case. This mobility was still high enough to push most of the protons through the membrane to the cathode, although the concentration decreases at the outer cathode boundary instead of increasing slightly as in the default case. The higher proton concentration in the membrane was enough to offset this slight decrease and yielded a 28.4% increase in hydrogen production over the default case.

4.5 Effects of Light

The anode and cathode electrode assemblies are composed of silicon and germanium to create a pn-junction (see Figure 1.3). As light strikes the cell, electrons are freed

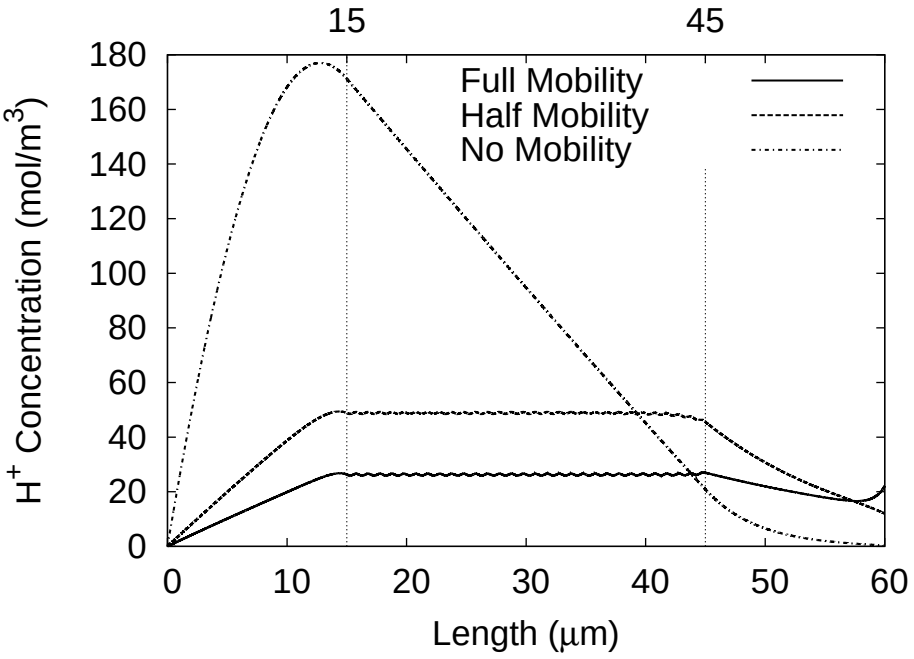

Figure 4.7: Concentration profile for full, half, and no mobility.

due to the photoelectric effect which causes a current to flow. Since the total current is assumed to be constant, an increase in photocurrent results in a decrease in the applied current. The overpotentials depend on the applied current, so the overpotentials decrease as the light irradiance increases, as found by Nie [4]. These results are shown in Figure 4.8(b) which reveals a lower applied potential for higher light irradiance. The change in electric potential also affects the hydrogen concentration as shown in Figure 4.8(a). The reduced electric potential causes a slight increase in hydrogen concentration. As expected, increasing the light irradiance while keeping the total current density constant reduces the required power density while also slightly increasing hydrogen production.

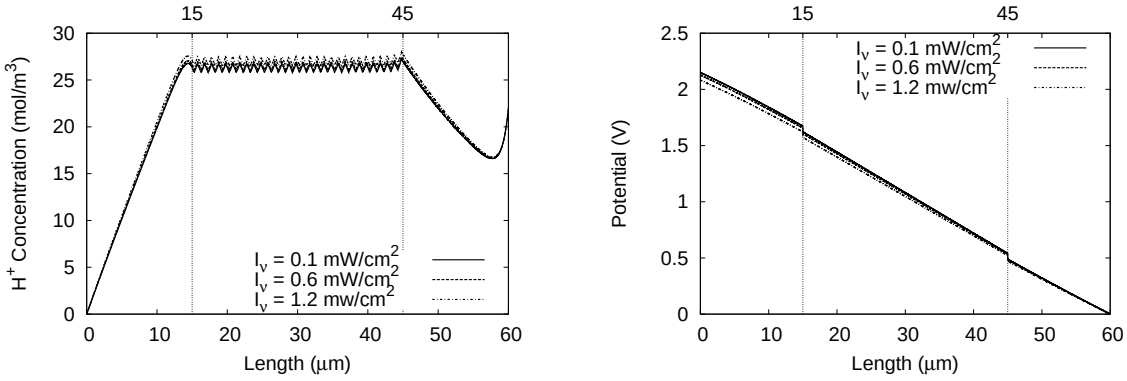

(a) Concentration

(b) Electric Potential

Figure 4.8: Concentration and electric potential profiles for light irradiances of I_ν =.1, .5, and .8 mW/cm^2.

4.6 Effects of Mass Transfer Coefficient

The mass transfer coefficient K_{MT} describes the rate by which protons pass through the cathode boundary to the water channel and depends on the rate of water flow through the water channel. For $K_{MT} = \infty$, the boundary condition forces the proton concentration to equal n_0 at the boundary, which corresponds to pH 7 (neutral). In this case, the flow of water through the water channel is very fast so that the boundary concentration is kept at that of bulk water. At the other extreme, for $K_{MT} = 0$ the boundary condition forces the flux of protons through the boundary

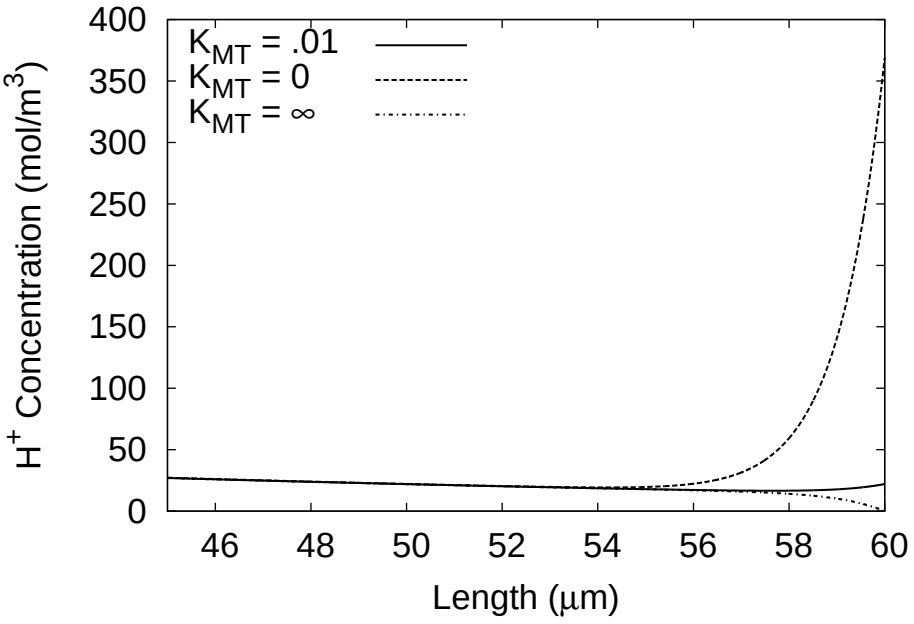

Figure 4.9: Concentration profile in the cathode for mass transfer coefficients of K_{MT} = 0, .01, and ∞.

to be zero which causes a pile-up of protons at the boundary. This condition over-estimates the hydrogen production by twice as much as the default case while the $K_{MT} = 0$ case under-estimates hydrogen production. For this reason, the default case is taken to be $K_{MT} = .01$ which is between the extreme cases. These three cases are shown in Figure 4.9.

4.7 Effects of Cell Size

In order for the PEM PEC to become a viable means of hydrogen production, vast amounts of hydrogen will need to be produced. This will require efficient production of the electrode regions of the cell without defects at much larger sizes than those used in our model [7, 8, 9]. The three main sizes which affect hydrogen production are the size of the electrodes, size of the membrane, and pitch between scaffolds.

The pitch refers to the distance between scaffolds in the electrode assembly (see Figure 2.4). The effects of a change in pitch are shown in Figure 4.10. The main effect of a decrease in pitch is the significant increase in hydrogen production due to a larger source for electrolysis. Electrolysis occurs on the surface of the electrodes on the platinum catalyst making surface area a critical parameter. An increase in pitch corresponds to more nanowires per unit area in the electrodes. This increases the surface area for electrolysis and hence greatly improves hydrogen production. To optimize the cell, a large surface area on the electrode assemblies is needed which can be accomplished by decreasing the pitch between nanowires.

Similar to the pitch, the length of the electrodes also plays an important role in

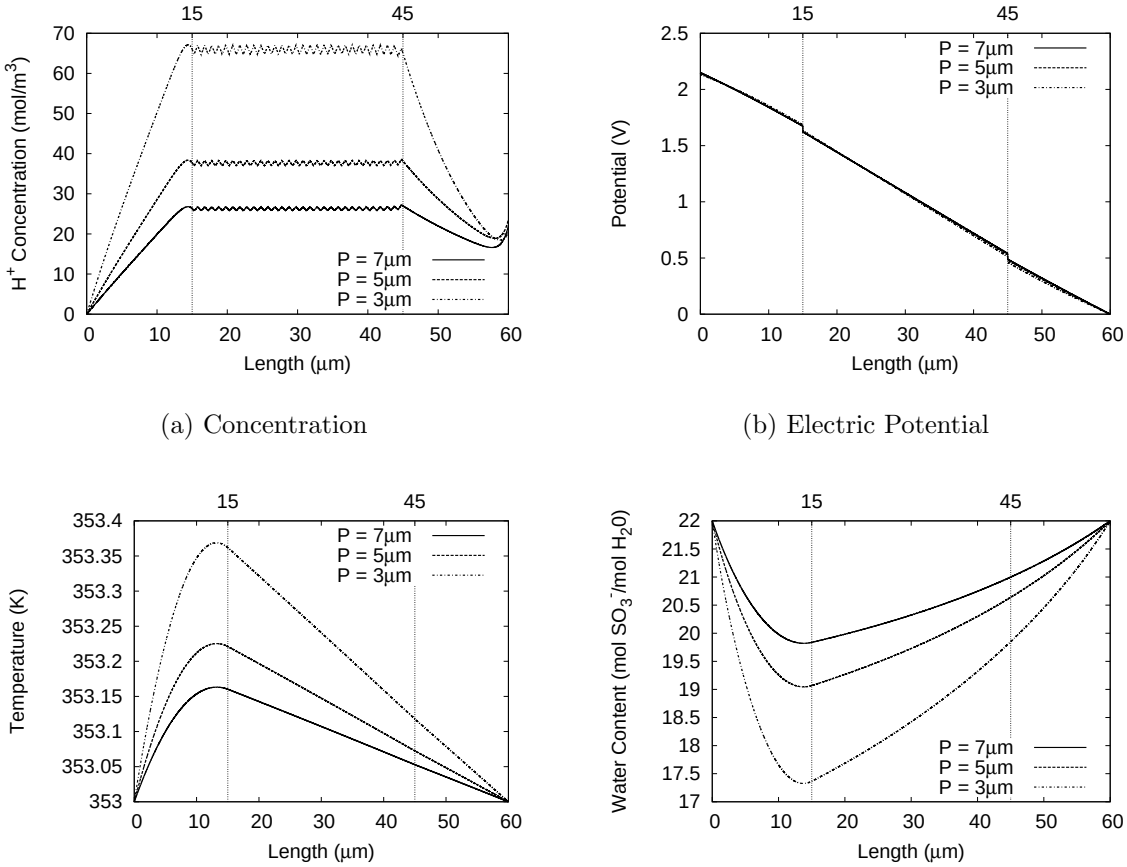

(a) Concentration

(b) Electric Potential

(c) Temperature

(d) Water Content

Figure 4.10: Pitch $P = 7\mu$m, 5μm, and 3μm.

hydrogen production due to changing the surface area available for electrolysis. By decreasing the size of both electrodes to 10μm as shown in Figure 4.11, the average proton concentration in the membrane decreases to about half of that for the default case causing hydrogen production to decrease to 41.4% of default. If the electrode length is increased to 30μm, however, the average proton concentration in the membrane increases significantly as seen in Figure 4.12 resulting in a 384.6% increase over

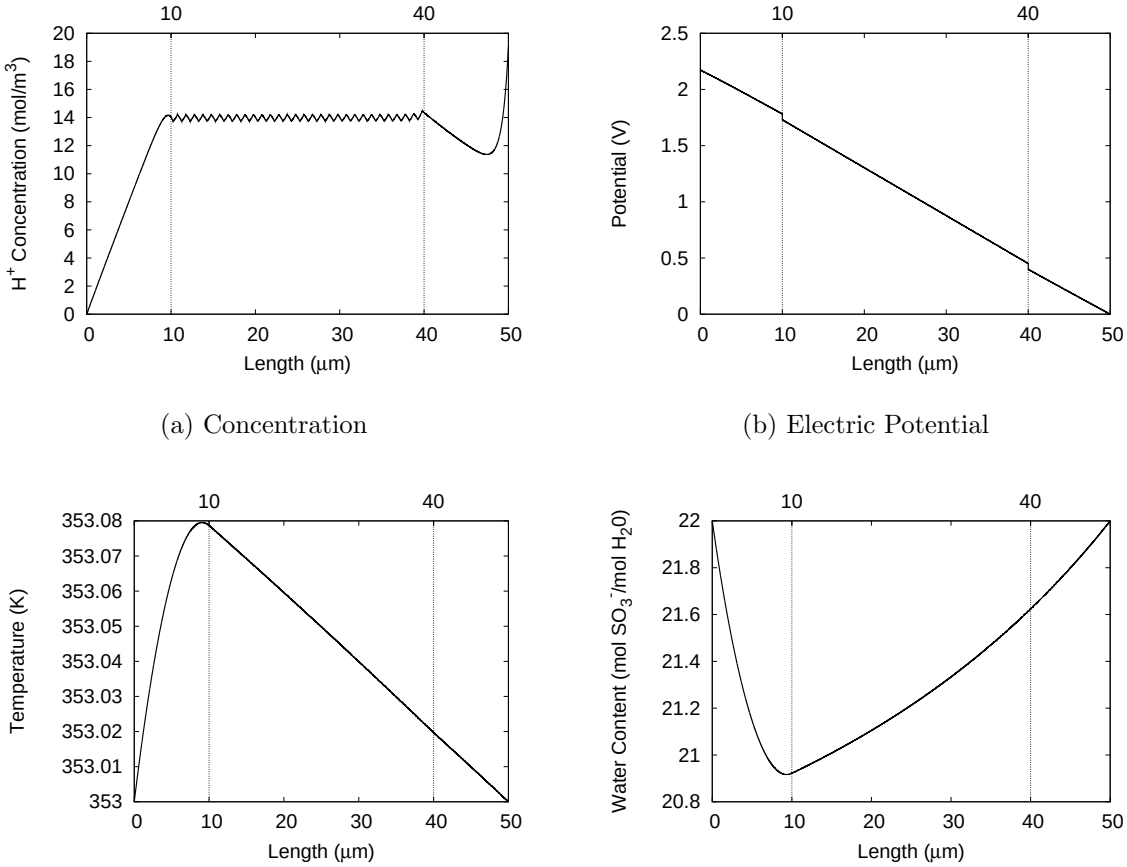

(a) Concentration

(b) Electric Potential

(c) Temperature

(d) Water Content

Figure 4.11: Electrode size $L_A = L_C = 10\mu$m.

default. An additional effect of an increase in electrode length is the decrease in water content in the central region of the cell. This decrease in water content causes less diffusivity as shown by equation 2.28 which aids in hydrogen production. These few cases illustrate the dramatic effect that the size of the electrodes have on hydrogen production.

Membrane size can also be varied, although the effects are not as extreme as those

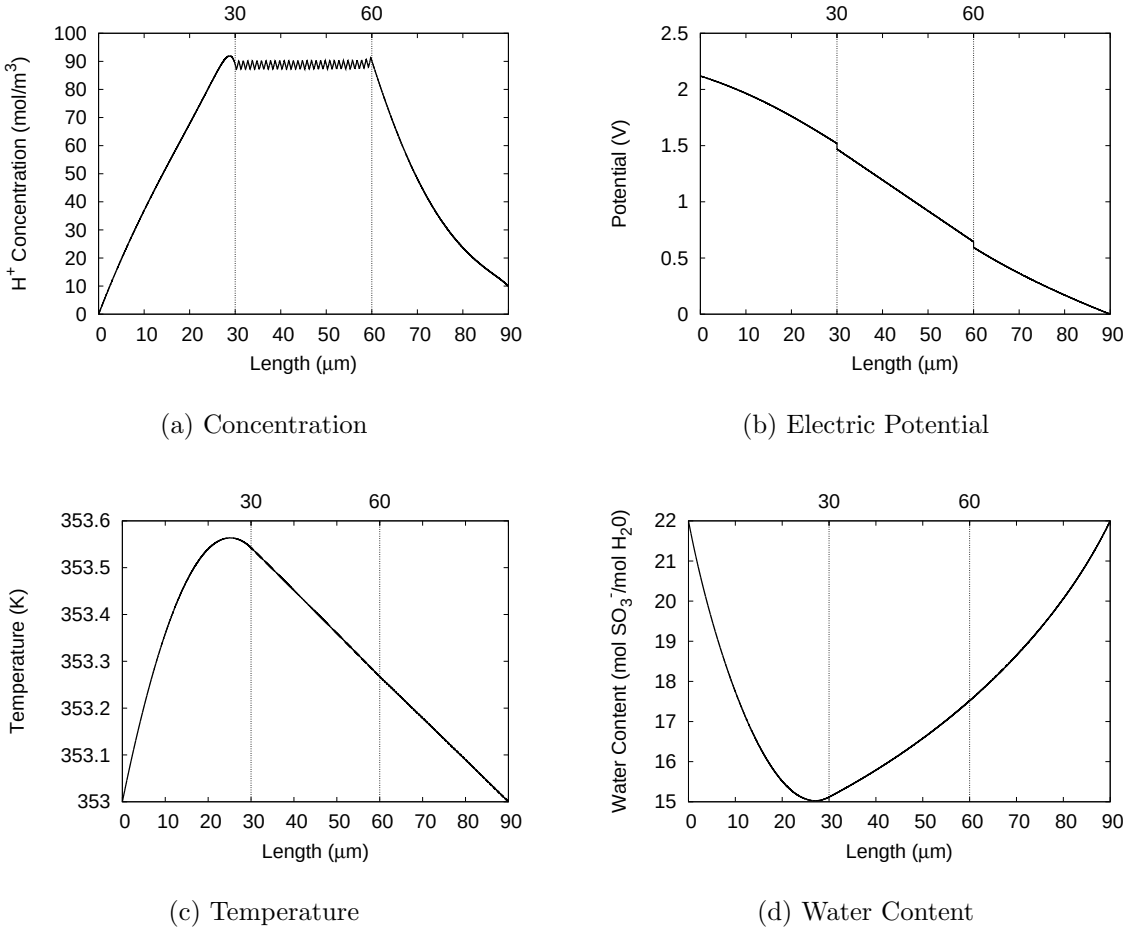

(a) Concentration

(b) Electric Potential

(c) Temperature

(d) Water Content

Figure 4.12: Electrode size $L_A = L_C = 30\mu$m.

for the electrodes. Figure 4.13 shows the results for a membrane length of 20μm while Figure 4.14 is for a 40μm long membrane. Almost counterintuitively, hydrogen production increases as the length of the membrane increases. The purpose of the membrane is simply to allow the protons to drift and diffuse through to the cathode and the only source present in the membrane is the delta functions for SO_3^- and H^+ charges, which have been shown to have little impact on hydrogen production. This

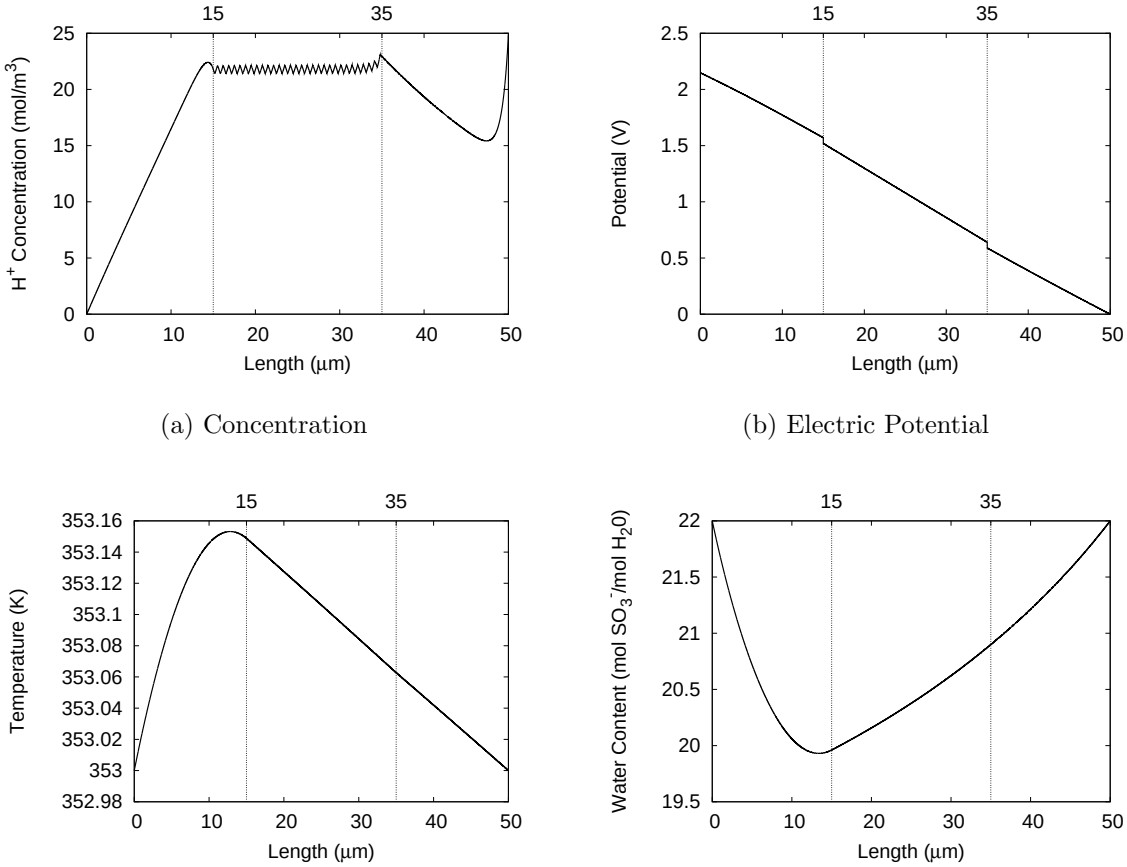

(a) Concentration

(b) Electric Potential

(c) Temperature

(d) Water Content

Figure 4.13: Membrane size $L_M = 20\mu$m.

thought process implies that a shorter membrane should operate more efficiently, however, this is not the case. As the drift and diffusion transport mechanisms act on the protons, a longer membrane allows more space for the protons to pile-up before combining to form H_2 gas. Concentration levels in the membrane are slightly higher for the 40μm case and slightly lower in the 20μm case. Higher concentration values yield more hydrogen production.

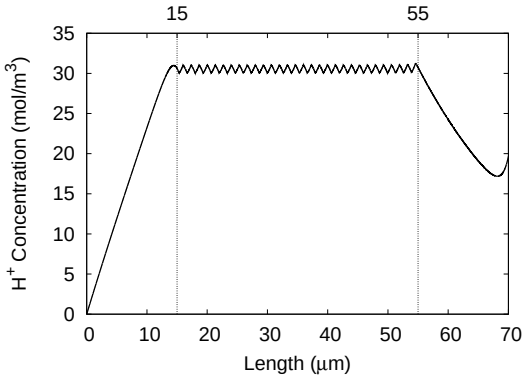

(a) Concentration

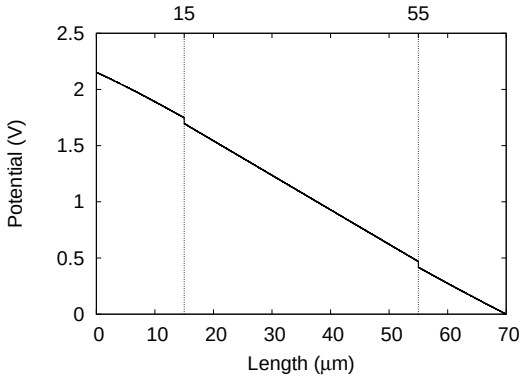

(b) Electric Potential

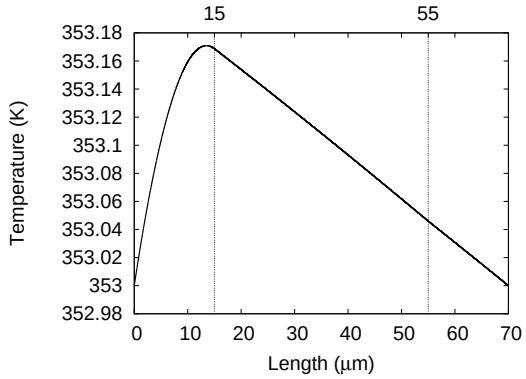

(c) Temperature

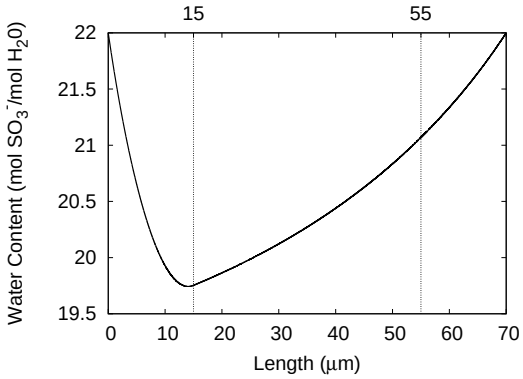

(d) Water Content

Figure 4.14: Membrane size $L_M = 40\mu$m.

CHAPTER V

CONCLUSIONS AND FUTURE WORK

By studying the effects of PEM PEC parameters, intuition can be gained on the processes involved in electrolyzing water to form hydrogen gas. Once produced, the hydrogen gas can be stored and used for fuel by using available fuel cells to convert the hydrogen gas to electric current. Cell parameters must be adjusted in order to increase the amount of hydrogen production so that the cells become an economic and efficient alternative to current fuel sources. Parameters which showed the most significant increases in hydrogen production are lengthening the electrodes to 30μm (384.6% increase), decreasing the pitch (305.8% increase), reducing the mass transfer coefficient between the cathode and water channel to zero (208.3% increase), and decreasing the input water concentration to $\lambda = 12$ (160.8% increase). Lengthening the electrodes and decreasing the pitch show the largest increases in production, which is expected. The longer electrodes allow a longer region for electrolysis at the anode and more area for hydrogen protons to be combined to form hydrogen gas at the cathode. In a similar manner, decreasing the pitch results in more surface area for the reactions to occur. The mass transfer coefficient also plays a large role in hydrogen production, although this parameter is difficult to adjust in applications. Production can also be increased by using an appropriate water content, although

caution must be used to avoid dehydration which would cause hydrogen production to nearly cease. Water content must be kept low enough to avoid saturation, yet high enough to avoid dehydration.

The work presented in this paper offers useful insight into the operation of the PEM PEC, although much more work must be done to fully optimize the cell so that the amount of hydrogen production offers an economical alternative to current fuel sources. Perhaps the most beneficial expansion to the current paper would be the inclusion of the water channels in the model. The proposed model accounts for some of the effects of the water channels in the outer boundary conditions, but more accurate results could be obtained by applying the governing equations along with appropriate source/sink terms and boundary conditions to the water channels. It should be noted that this would also increase the computational expense considerably since the water channels are several times larger than the anode, membrane, and cathode.

Another possible expansion would be to use a multi-dimensional model instead of the proposed one-dimensional model. This would allow a more accurate model of the charge groups in the membrane as well as include effects of all cell boundaries. To improve the model, nonlinear channel flow could be considered as well. In the current model, protons are assumed to flow linearly from anode to cathode, although the path is highly tortuous, especially in the membrane which is in fact a complex polymer structure [5]. Also, this paper only studied cases of evenly distributed charge groups which is not always the case in Nafion.

As found in Section 4.4, the mobility of protons can have unexpected results on

hydrogen production. The half mobility case actually increased hydrogen production due to a pile-up of protons in the membrane. A more detailed approach is needed to determine the most effective mobility.

One final generalization would be a transient analysis of the cell. Only steady-state conditions are studied in the proposed model. The transient response could be derived from the governing equations provided in this paper and could yield insight into the start-up behavior of the cell.

In conclusion, much more work is still needed before the PEM PEC is an economic alternative to natural fuels, although this paper offers insight into the operation and distributions throughout the cell. By adjusting cell parameters, a cell is shown to theoretically produce up to 22.5 ml/min of hydrogen gas to be used for fuel.

BIBLIOGRAPHY

[1] J. Adams. A Homogenization Model of a Proton Exchange Membrane Photoelectrochemical Cell. *Masters Thesis, The University of Akron*, 2010.

[2] J.M. Ogden. Hydrogen: The fuel of the future? *Physics Today*, 55(4):69–75, APR 2002.

[3] K.A. Adamson. Hydrogen from renewable resources - the hundred year commitment. *Energy Policy*, 32(10):1231–1242, JUL 2004.

[4] J. Nie, Y. Chen, R.F. Boehm, and S. Katukota. A photoelectrochemical model of proton exchange water electrolysis for hydrogen production. *Journal of Heat Transfer-Transactions of the ASME*, 130(4), APR 2008.

[5] Y. Akinaga, S. Hyodo, and T. Ikeshoji. Lattice Boltzmann simulations for proton transport in 2-D model channels of Nafion. *Physical Chemistry Chemical Physics*, 10(37):5678–5688, 2008.

[6] J.A. Elliott and S.J. Paddison. Modelling of morphology and proton transport in PFSA membranes. *Physical Chemistry Chemical Physics*, 9(21):2602–2618, JUN 7 2007.

[7] B.M. Kayes, M.A. Filler, M.C. Putnam, M.D. Kelzenberg, N.S. Lewis, and H.A. Atwater. Growth of vertically aligned Si wire arrays over large areas (> 1 cm^2) with Au and Cu catalysts. *Applied Physics Letters*, 91(10), SEP 3 2007.

[8] J.R. Maiolo III, B.M. Kayes, M.A. Filler, M.C. Putnam, M.D. Kelzenberg, H.A. Atwater, and N.S. Lewis. High aspect ratio silicon wire array photoelectrochemical cells. *Journal of the American Chemical Society*, 129(41):12346+, OCT 17 2007.

[9] J.M. Spurgeon, S.W. Boettcher, M.D. Kelzenberg, B.S. Brunschwig, H.A. Atwater, and N.S. Lewis. Flexible, Polymer-Supported, Si Wire Array Photoelectrodes. *Advanced Materials*, 22(30):3277+, AUG 10 2010.

[10] C.Y. Du, X.Q. Cheng, T. Yang, G.P. Yin, and P.F. Shi. Numerical simulation of the ordered catalyst layer in cathode of Proton Exchange Membrane Fuel Cells. *Electrochemistry Communications*, 7(12):1411–1416, DEC 2005.

[11] K.J. Lee, J.H. Nam, and C.J. Kim. Steady saturation distribution in hydrophobic gas-diffusion layers of polymer electrolyte membrane fuel cells: A pore-network study. *Journal of Power Sources*, 195(1):130–141, JAN 1 2010.

[12] K. Kang and H. Ju. Numerical modeling and analysis of micro-porous layer effects in polymer electrolyte fuel cells. *Journal of Power Sources*, 194(2, Sp. Iss. SI):763–773, DEC 1 2009.

[13] F. Chen, M.H. Chang, and C.F. Fang. Analysis of water transport in a five-layer model of PEMFC. *Journal of Power Sources*, 164(2):649–658, FEB 10 2007.

[14] K.D. Kreuer. On the development of proton conducting polymer membranes for hydrogen and methanol fuel cells. *Journal of Membrane Science*, 185(1, Sp. Iss. SI):29–39, APR 15 2001.

[15] E. Afshari and S.A. Jazayeri. Analyses of heat and water transport interactions in a proton exchange membrane fuel cell. *Journal of Power Sources*, 194(1, Sp. Iss. SI):423–432, OCT 20 2009. 10th Symposium on Fast Ionic Conductors, Grybow, POLAND, SEP 14-17, 2008.

[16] C.Y. Wang. Fundamental models for fuel cell engineering. *Chemical Reviews*, 104(10):4727 – 4766, 2004.

APPENDIX

HOMOGENIZATION

This appendix shows the details of the homogenization process for the PEM PEC. We begin with Gauss's law in two-dimensions,

$$\Phi_{xx} + \Phi_{yy} + \frac{\rho}{\epsilon} = 0. \tag{A.1}$$

Integrating in the y-direction over the length of the pitch and pitch of the scaffold (see Figure 2.4) we find

$$\int_0^{P+P_{\text{scaffold}}} \left(\Phi_{xx} + \Phi_{yy} + \frac{\rho}{\epsilon}\right) \mathrm{d}y = 0. \tag{A.2}$$

No potential or electric charge is present in the scaffold since the scaffolds are composed of Si and Ge which are conductors. This simplifies the equation to

$$\int_0^{P} \left(\Phi_{xx} + \Phi_{yy} + \frac{\rho}{\epsilon}\right) \mathrm{d}y = 0. \tag{A.3}$$

Between scaffolds is bulk water at pH 7. There is no space charge density for neutral water, so $\rho = 0$, which gives

$$\int_0^{P} \left(\Phi_{xx} + \Phi_{yy}\right) \mathrm{d}y = 0. \tag{A.4}$$

Performing the integration we find

$$P\Phi_{xx} + \Phi_y \Big|_0^P = 0. \tag{A.5}$$

The boundary condition is given by Ohm's law, which states that

$$\begin{aligned} \vec{J} &= \sigma \vec{E} \\ &= -\sigma \frac{\partial \Phi}{\partial \hat{n}}, \end{aligned} \tag{A.6}$$

where $\hat{n}$ is a unit vector normal to the surface. Applying the boundary condition to equation (A.5) we obtain

$$P\Phi_{xx} + \left[\frac{J}{\sigma} - \left(-\frac{J}{\sigma}\right)\right] = 0. \tag{A.7}$$

We let $A = \frac{2}{P}$, resulting in

$$\begin{aligned} \Phi_{xx} &= -\frac{J}{\frac{1}{2}P\sigma} \\ &= -\frac{JA}{\sigma}, \end{aligned} \tag{A.8}$$

which is a one-dimensional equivalent of equation (2.10). Thus, the surface area/volume ratio of the electrodes is given by $A = \frac{2}{P}$ in order to create a one-dimensional homogenized model of the PEM PEC.